

Non-Perturbative Study of the Light Pseudoscalar Masses in Chiral Dynamics

José A. Oller^{#1} and Luis Roca^{#2}

*Departamento de Física. Universidad de Murcia.
E-30071 Murcia. Spain.*

Abstract

We perform a non-perturbative chiral study of the masses of the lightest pseudoscalar mesons. The pseudoscalar self-energies are calculated by the evaluation of the scalar self-energy loops with full S-wave meson-meson amplitudes taken from Unitary Chiral Perturbation Theory (UCHPT). These amplitudes, among other features, contain the lightest nonet of scalar resonances σ , $f_0(980)$, $a_0(980)$ and κ . The self-energy loops are regularized by a proper subtraction of the infinities within a dispersion relation formulation of the scattering amplitudes. Values for the bare masses of pions and kaons are obtained as well as an estimate of the mass of the η_8 . We then match to the self-energies from standard Chiral Perturbation Theory (CHPT) to $\mathcal{O}(p^4)$ and resum higher orders from our calculated scalar self-energies. The dependence of the self-energies on the quark masses allows a determination of the ratio of the strange quark mass over the mean of the lightest quark masses, m_s/\hat{m} , in terms of the $\mathcal{O}(p^4)$ CHPT low energy constant combinations $2L_8^r - L_5^r$ and $2L_6^r - L_4^r$. In this way, we give a range for the values of these low energy counterterms and for $3L_7 + L_8^r$, once the η meson mass is invoked. The low energy constants are further constraint by performing a fit to the recent MILC lattice data on the pseudoscalar masses. An excellent reproduction of the MILC data is obtained, at the level of 1% of relative error in the pseudoscalar masses, and $m_s/\hat{m} = 25.6 \pm 2.5$ results. This value is consistent with 24.4 ± 1.5 from CHPT and phenomenology and more marginally with the value 27.4 ± 0.5 obtained from pure perturbative chiral extrapolations of the MILC lattice data to physical values of the lightest quark masses.

arXiv:hep-ph/0608290v1 28 Aug 2006

^{#1}email: oller@um.es

^{#2}email: luisroca@um.es

1 Introduction

Chiral Perturbation Theory (CHPT) is the effective quantum field theory of strong interactions at low energies [1, 2, 3]. Three flavour CHPT, including strangeness, has already reached a very sophisticated stage with present calculations at the level of next-to-next-to-leading order (NNLO) or $\mathcal{O}(p^6)$ [4, 5, 6]. In ref.[7] the masses and decay constants of the lightest octet of pseudoscalar mesons are worked out at NNLO. One striking fact concerns the much larger $\mathcal{O}(p^6)$ two loop contribution than the full $\mathcal{O}(p^4)$ one to the selfenergies of the pseudoscalars, by around one order of magnitude. In addition, for the kaon and eta masses, the $\mathcal{O}(p^6)$ tree level contributions, with the $\mathcal{O}(p^6)$ chiral counterterms estimated by resonance saturation, are very large in modulus, by several factors, than the $\mathcal{O}(p^6)$ pure loop ones and with opposite sign. As stated in ref.[7] the $\mathcal{O}(p^6)$ counterterms “seem severely overestimated” due to the complicated nature of the scalar sector and how these contributions are evaluated there. Hence, this study rises the interesting question of how one can improve the calculation of the contributions from the scalar sector. This is an object of study of the present investigation.

Concerning again the importance of the S-wave dynamics, it is well known that the scalar sector is the source of large higher order corrections to the CHPT series, because of the enhancement of unitarity diagrams, which definitely slow down the convergence of the perturbative chiral series. As a relevant example, let us quote the I=0 $\pi\pi$ scattering length, a_0^0 , which receives very large higher order corrections (a 40% correction with respect to the lowest order value). This is more dramatic if it is compared with the *non-resonant* I=2 S-wave scattering length, a_0^2 , which has negligible higher order corrections [8, 9, 10]. Even larger higher order chiral corrections due to the I=0 S-wave final state interactions happen for the lowest order prediction of $\Gamma(\eta \rightarrow 3\pi)$, more than a factor of 2 [11, 12]. In connection with these enhancements, because of the self-interactions among the pseudoscalars in S-wave, one has the *generation* of the lightest scalar resonances σ , $f_0(980)$, $a_0(980)$ and κ [13, 14, 15, 16], which are not included as explicit degrees of freedom but appear as poles in unphysical Riemann sheets of the partial wave scattering amplitudes. Another novel example, where these large corrections play a role, as we show in this work, concerns the determinations of the light quark masses from present lattice calculations of the pseudoscalar masses [17, 18, 19] with three dynamical fermions. In these evaluations lattice results are taken down to the physical values of the lightest quark masses, m_u and m_d , by employing pure perturbative SU(3) Staggered CHPT calculations [20], even though one confronts with the problematic S-wave dynamics plagued of non-perturbative effects. In addition, in SU(3) chiral dynamics one also has the issue of the much larger value of the s quark mass, m_s , with the associated large masses of kaons and etas. In this respect, the MILC Collaboration reports a value for the ratio $m_s/\hat{m} = 27.4 \pm 0.5$, with $\hat{m} = (m_u + m_d)/2$, inconsistent with its determination from CHPT and phenomenology [21], $m_s/\hat{m} = 24.4 \pm 1.5$. Here, m_u , m_d and m_s are the masses of the up, down and strange quarks, respectively. Because Unitary CHPT (UCHPT) has proved very successful in dealing, precisely, with the strong meson-meson S-wave interactions, it is worth employing this scheme as a parameterization to bring down the results from lattice QCD to the physical lightest quark masses and check whether this disagreement between lattice QCD and CHPT can be understood better. Here we will employ $\mathcal{O}(p^4)$ CHPT and supply it with the corrections from UCHPT of $\mathcal{O}(p^6)$ and higher. This has proved already very successful in many other processes like e.g. meson-meson scattering [13, 22, 15], $\gamma\gamma \rightarrow$ meson-meson [23], meson form factors [24, 25, 26], ϕ [27], J/Ψ [24, 28], η [29], B [30] and D [31] decays, determinations of light quark masses and V_{us} [32], etc. The point of considering our S-wave amplitudes, is because the right hand or unitarity cut is resummed, and then one takes care of such enhancements as well as of the contributions to the self energies due to the σ , $f_0(980)$, $a_0(980)$ and κ resonances. Indeed both effects are all intrinsically the same. One should remark that the generation of these resonances in SU(3) is not due to the largeness of the strange quark mass. This generation for the σ resonance already occurs in the SU(2) case, with only

pions. It also occurs even in the chiral limit, where a nonet of light scalar resonances, with properties of mass and width similar to those of the actual σ meson, is generated [14].

The manuscript is organized as follows. Section 2 is dedicated to the development of the formalism for the calculation of the self-energies and evaluation of the proper loop integrals. In section 3 the results without matching with CHPT at $\mathcal{O}(p^4)$ are given, this is what we call full dynamical self-energies. In this section we will provide a first approximation to the values of the bare pseudoscalar masses and to the m_s/\hat{m} ratio. In section 4 the $\mathcal{O}(p^4)$ CHPT self-energies are introduced and supplemented with higher order corrections from our formalism. Restrictions on the values of several combinations of CHPT low energies constants (LECs) are obtained from present determinations of m_s/\hat{m} . In section 5 we parametrize the MILC lattice QCD data on the pseudoscalar masses as a function of the quark masses, with a reproduction of the lattice data at the level of around 1%, and predict more constraint values for CHPT LECs and m_s/\hat{m} . We also compare with other determinations. In section 6 we summarize our results and conclusions.

2 Formalism

Our starting point is the S-wave meson-meson partial waves both for resonant isospins (I)=0, 1, 1/2 as well as for the much smaller and non-resonant ones, I=3/2 and 2. For the former set we take the amplitudes of ref.[14]. The interaction kernel employed in this reference comprises the lowest order CHPT amplitudes together with the exchange of s-channel scalar resonances in a chiral symmetric invariant way from ref.[33]. These tree level resonances constitute an octet with mass around 1.4 GeV and a singlet with mass around 1 GeV. On the other hand, the coupled channels are $\pi\pi$, $K\bar{K}$ and $\eta\eta$ for I=0, $\pi\eta$ and $K\bar{K}$ for I=1 and $K\pi$ and $K\eta$ for I=1/2. In addition to the resonances explicitly included at tree level, related to the physical ones around 1.4 GeV like e.g. the $K_0^*(1410)$ or the $a_0(1450)$, the approach also generates dynamically the σ or $f_0(600)$, κ , $a_0(980)$ resonances and the main contribution to the $f_0(980)$ one. These resonances are generated even when no explicit resonances at tree level are included and one then obtains a good reproduction of the data for energies below 1.2 GeV [13, 14].^{#3}The basic point in UCHPT is to resum the right hand or unitarity cut to all orders, the source of the large corrections produced by the S-wave meson-meson interactions, and perform a chiral expansion of the rest, the so called interaction kernel, calculating it perturbatively from CHPT [35, 36, 14]. For the non-resonant isospins 3/2 and 2, not given in ref.[14], we take the kernels for UCHPT at lowest order, that is, the $\mathcal{O}(p^2)$ CHPT amplitudes. In fig.1 we show the typical quality in the reproduction of the experimental data by the amplitudes that we use as input in the calculation of the self-energies.

We only consider the S-waves since the lightest pseudoscalar self-energies are expected to be dominated by low energy physics where the P-waves are kinematically suppressed by small factors of three-momentum squared. This is true even in the calculations of loops since then, after proper renormalization, the typical momentum in virtual processes will be bounded and of the same order as the on-shell values. Indeed, by a comparison of the order of magnitude of our results with those obtained by regularizing the loops with a three-momentum cut-off, the latter must be around 0.4-0.5 GeV. At such energies only S-waves matters in very good approximation, which is also clear experimentally. Another signal of the suppression of P-wave dynamics in self-energies is the fact that it only starts to contribute at the two chiral loop level. In addition, we recall the discussion in section 1 concerning the fact that the main source for large higher orders corrections for the chiral expansion, even at low energy, happens from

^{#3}When the $\eta\eta$ channel is also taken into account for the I=0 S-wave, together with the $\pi\pi$ and $K\bar{K}$ channels, the $(1-\eta^2)/4$ data are not properly reproduced unless an explicit singlet around 1 GeV is included [14]. However, as stated in the PDG [34], these data can have much larger uncertainties than the sizes of the given errors.

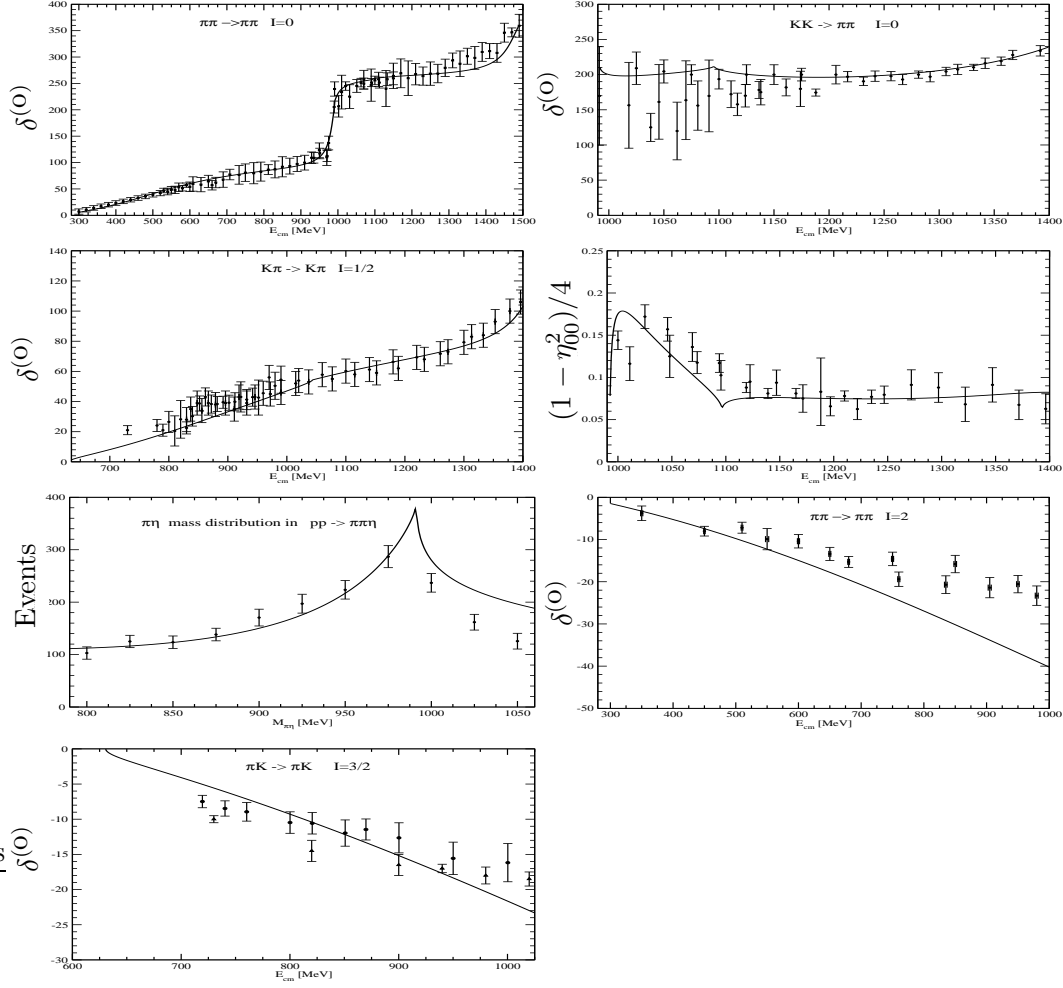


Figure 1: Different phase-shifts, inelasticities and mass distributions obtained with the unitarized amplitudes. The experimental data are from refs. [37, 38, 39, 40, 41, 42, 43, 44, 45, 46, 47, 48, 49]

the strong meson-meson S-wave interactions in the resonant isospin channels, and our aim is to provide an estimation of such large effects, relying in the chiral expansion for other contributions that can be calculated perturbatively.

2.1 Expression for the self-energy

The set of diagrams enhanced in S-wave meson-meson scattering are represented in fig.2a, for the process $P\bar{Q} \rightarrow P\bar{Q}$. Now, we want to calculate the contribution to the pseudoscalar self-energies from these enhanced diagrams. The solution is transparent from the diagrammatic point of view, fig.2b. It consists of joining an initial and a final Q external line in the S-wave $P\bar{Q} \rightarrow P\bar{Q}$ amplitude in fig.2a and summing over all $Q = \{\pi^+, \pi^-, \pi^0, K^+, K^-, K^0, \bar{K}^0, \eta\}$. Notice that the directions of the arrows for the Q pseudoscalar are reversed compared to the \bar{Q} ones in fig.2a.

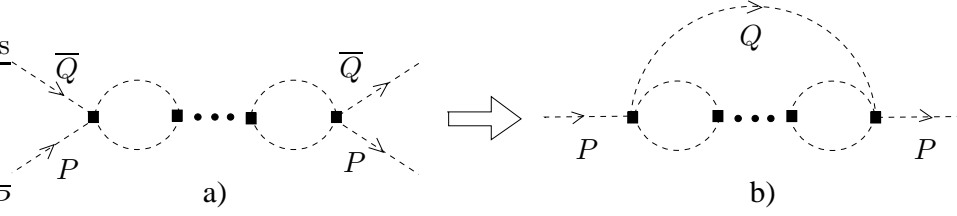


Figure 2: Fig.2a represents the S-wave amplitude $P\bar{Q} \rightarrow P\bar{Q}$ and fig.2b is the diagram for the calculation of the self-energy of the pseudoscalar P due to the intermediate pseudoscalar Q .

The evaluation of the diagram fig.2b can be better recast as in fig.3. In this figure the pseudoscalar field P enters with an arbitrary four momentum p and the filled circles correspond to the full $P \rightarrow Q_1 Q_2 Q_3$ amplitude. Applying the Cutkowsky rules one can evaluate the discontinuity of this diagram due to the branch cut originated by putting on-shell the three intermediate pseudoscalars Q_1 , Q_2 and Q_3 ,

$$\Delta F_1 = - \int \frac{d^3 q}{(2\pi)^3 2E_{Q_1}(\mathbf{q})} \left[i \int \frac{d^3 k (2\pi) \delta(p^0 - E_{Q_1} - E_{Q_2} - E_{Q_3})}{(2\pi)^3 2E_{Q_2}(\mathbf{k}) 2E_{Q_3}(\mathbf{q} + \mathbf{k})} T(P \rightarrow Q_1 Q_2 Q_3)^* T(Q_1 Q_2 Q_3 \rightarrow P) \right], \quad (2.1)$$

where $E_{Q_i}(\mathbf{p}) = \sqrt{M_{Q_i}^2 + \mathbf{p}^2}$.

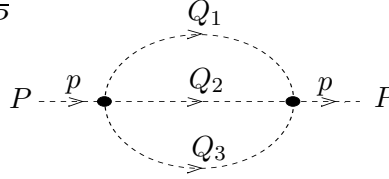


Figure 3: Self-energy diagram. P is the incident pseudoscalar with arbitrary timelike four-momentum p and Q_1 , Q_2 and Q_3 are the intermediate pseudoscalars. The filled circles correspond to the full $P \leftrightarrow Q_1 Q_2 Q_3$ amplitudes.

Now, the expression between brackets is nothing else but the unitarity condition for the $P\bar{Q}_1 \rightarrow P\bar{Q}_1$ amplitude due to the intermediate $(Q_2 Q_3)$ state. This condition determines the discontinuity of a physical amplitude across the right hand or unitarity cut. Of course, there is still an integration over \vec{q} since one must sum over all the intermediate momentum-defined on-shell states of the pseudoscalar Q_1 . This is what we meant above by joining the Q lines in the $P\bar{Q} \rightarrow P\bar{Q}$ S-wave amplitude. The discontinuity shown in eq.(2.1) is the right hand cut present in the $P\bar{Q}_1 \rightarrow P\bar{Q}_1$ S-wave amplitude calculated for arbitrary timelike p . And hence,

$$- \int \frac{d^3 q}{(2\pi)^3 2E_{Q_1}(\mathbf{q})} T(P\bar{Q}_1 \rightarrow P\bar{Q}_1), \quad (2.2)$$

has the same discontinuity as that of eq.(2.1), with T calculated within our scheme having only the right hand cut. Notice that we have made use of crossing for relating $T(P \rightarrow Q_1 Q_2 Q_3)$ with $T(P\bar{Q}_1 \rightarrow Q_2 Q_3)$.

Next, we could reorder the labels of the intermediate pseudoscalars in fig.3 and recast eq.(2.1) in two more forms,

$$\Delta F_2 = - \int \frac{d^3 q}{(2\pi)^3 2E_{Q_2}(\mathbf{q})} \left[i \int \frac{d^3 k (2\pi) \delta(p^0 - E_{Q_1} - E_{Q_2} - E_{Q_3})}{(2\pi)^3 2E_{Q_1}(\mathbf{k}) 2E_{Q_3}(\mathbf{q} + \mathbf{k})} T(P \rightarrow Q_1 Q_2 Q_3)^* T(Q_1 Q_2 Q_3 \rightarrow P) \right], \quad (2.3)$$

and

$$\Delta F_3 = - \int \frac{d^3 q (2\pi)}{(2\pi)^3 2E_{Q_3}(\mathbf{q})} \left[i \int \frac{d^3 k (2\pi) \delta(p^0 - E_{Q_1} - E_{Q_2} - E_{Q_3})}{(2\pi)^3 2E_{Q_1}(\mathbf{k}) 2E_{Q_2}(\mathbf{q} + \mathbf{k})} T(P \rightarrow Q_1 Q_2 Q_3)^* T(Q_1 Q_2 Q_3 \rightarrow P) \right]. \quad (2.4)$$

The expressions closed between brackets correspond to the unitarity cuts of $P\bar{Q}_2 \rightarrow P\bar{Q}_2$ and $P\bar{Q}_3 \rightarrow P\bar{Q}_3$, due the intermediate states $(Q_1 Q_3)$ and $(Q_1 Q_2)$, respectively. For different Q_i , none of these cuts are included in eq.(2.2) because our amplitudes are not crossing symmetric. However, we can calculate $P\bar{Q}_2 \rightarrow P\bar{Q}_2$ and $P\bar{Q}_3 \rightarrow P\bar{Q}_3$, in the same way as $P\bar{Q}_1 \rightarrow P\bar{Q}_1$, with the appropriate unitarity cuts of eqs.(2.3) and (2.4). If some of the Q_i are equal then we must not sum twice since the discontinuity is already taken into account. Then our expression for the self energy of the pseudoscalar P due to the loops schematically represented in fig.3 is given by the sum,

$$\Sigma_P^U = - \sum_Q \int \frac{d^3 k}{(2\pi)^3 2E_Q(\mathbf{k})} T_{P\bar{Q} \rightarrow P\bar{Q}}(s_1), \quad (2.5)$$

with $Q = \{\pi^+, \pi^-, \pi^0, K^+, K^-, K^0, \bar{K}^0, \eta\}$ and $s_1 = (M_P - E_Q(\mathbf{k}))^2 - \mathbf{k}^2$ for $p = (M_P, \vec{0})$. Of course, the previous equation is invariant under Lorentz transformation as must be the case for a self-energy because a meson-meson scattering amplitude is a Lorentz scalar. The sum in eq.(2.5) is over all the species of pseudoscalars because all of them give rise to different $P\bar{Q}_i \rightarrow P\bar{Q}_i$ amplitudes.

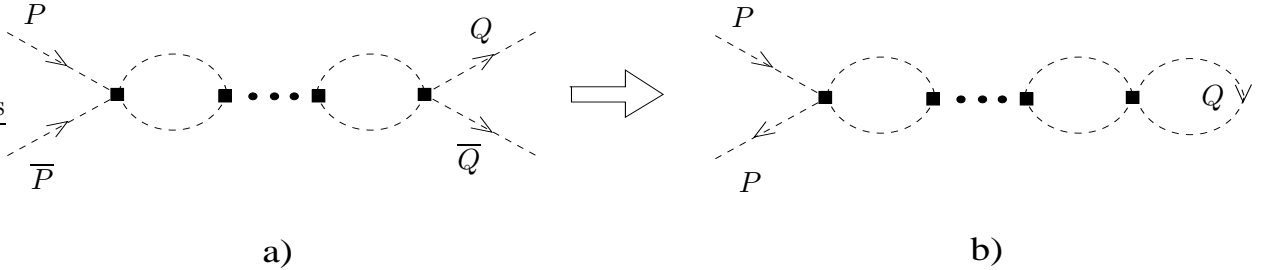


Figure 4: Tadpole diagram for the self-energy of the pseudoscalar P .

Diagrammatically it is clear that apart from fig.2 one should consider the crossed process in which the two P 's appear on the same side of the diagram, as shown in fig.4. Notice that in fig.3 we were driven to consider the amplitudes $P\bar{Q}_i \rightarrow P\bar{Q}_i$, but one also has the t -crossed process $P\bar{P} \rightarrow Q_i\bar{Q}_i$ that should be taken into account. Hence, we finally have a new expression analogue to eq.(2.5) but with $P\bar{P}$ as initial state and with $s_1 = 0$. This is a tadpole contribution without flow of four-momentum running through the loops,

$$\Sigma_P^{tad} = - \sum_{Q=\pi^0, \pi^+, K^+, K^0} \lambda_Q \int \frac{d^3 k}{(2\pi)^3 2E_Q(\mathbf{k})} T_{P\bar{P} \rightarrow Q\bar{Q}}(0). \quad (2.6)$$

In Σ_P^{tad} one sums only over particles (without including the sum over antiparticles) since in the final state both particles and antiparticles happen and otherwise one is double-counting. Finally, $\lambda_Q = 1$ for π^+ , K^+ and K^0 and $\lambda_Q = 1/2$ for π^0 and η , because they are their own antiparticles. These warnings also happen in the standard calculations of tadpoles with the use of Feynman rules because of the same reasons.

Our final result for the self-energy of the pseudoscalar P is the sum,

$$\Sigma_P = \Sigma_P^U + \Sigma_P^{tad} , \quad (2.7)$$

with Σ_P^U given in eq.(2.5) and Σ_P^{tad} in eq.(2.6). In particular, in terms of the amplitudes for the different channels we have, for π , K and η ,

$$\begin{aligned} \Sigma_\pi &= - \int \frac{d^3 k}{(2\pi)^3 2E_Q(\mathbf{k})} \left[\frac{10}{3} T_{\pi\pi \rightarrow \pi\pi}^{I=2}(s) + \frac{2}{3} T_{\pi\pi \rightarrow \pi\pi}^{I=0}(s) + \frac{8}{3} T_{\pi\bar{K} \rightarrow \pi\bar{K}}^{I=3/2}(s) + \frac{4}{3} T_{\pi\bar{K} \rightarrow \pi\bar{K}}^{I=1/2}(s) + T_{\pi\eta \rightarrow \pi\eta}^{I=1}(s) \right. \\ &\quad \left. + T_{\pi\pi \rightarrow \pi\pi}^{I=0}(0) + \frac{2}{\sqrt{3}} T_{\pi\pi \rightarrow K\bar{K}}^{I=0}(0) - \frac{1}{\sqrt{3}} T_{\pi\pi \rightarrow \eta\eta}^{I=0}(0) \right] \\ \Sigma_K &= - \int \frac{d^3 k}{(2\pi)^3 2E_Q(\mathbf{k})} \left[2T_{\pi K \rightarrow \pi K}^{I=3/2}(s) + T_{\pi K \rightarrow \pi K}^{I=1/2}(s) + \frac{3}{2} T_{K\bar{K} \rightarrow K\bar{K}}^{I=1}(s) + \frac{1}{2} T_{K\bar{K} \rightarrow K\bar{K}}^{I=0}(s) \right. \\ &\quad \left. + \frac{3}{2} T_{K\bar{K} \rightarrow KK}^{I=1}(s) + \frac{1}{2} T_{K\bar{K} \rightarrow KK}^{I=0}(s) + T_{K\eta \rightarrow K\eta}^{I=1/2}(s) \right. \\ &\quad \left. + \frac{\sqrt{3}}{2} T_{K\bar{K} \rightarrow \pi\pi}^{I=0}(0) + T_{K\bar{K} \rightarrow K\bar{K}}^{I=0}(0) - \frac{1}{2} T_{K\bar{K} \rightarrow \eta\eta}^{I=0}(0) \right] \\ \Sigma_\eta &= - \int \frac{d^3 k}{(2\pi)^3 2E_Q(\mathbf{k})} \left[3T_{\pi\eta \rightarrow \pi\eta}^{I=1}(s) + 4T_{\eta K \rightarrow \eta K}^{I=1/2}(s) + 2T_{\eta\eta \rightarrow \eta\eta}^{I=0}(s) \right. \\ &\quad \left. - \sqrt{3} T_{\eta\eta \rightarrow \pi\pi}^{I=0}(0) - 2T_{\eta\eta \rightarrow K\bar{K}}^{I=0}(0) + T_{\eta\eta \rightarrow \eta\eta}^{I=0}(0) \right] \end{aligned} \quad (2.8)$$

One remarkable fact of eqs.(2.5) and (2.6) is that the strong amplitude appears on-shell so that we can employ our previously calculated strong T-matrices evaluated on-shell, and well confronted with experiment. For the T_{ij} amplitude, for channel i going to channel j , we will restrict ourselves to the S-waves since they are the aim of our study because they are enhanced for $I=0, 1$ and $1/2$, as previously remarked.

The integral in eq.(2.5) for Σ_P^U is ultraviolet divergent since for large three-momentum the measure grows as \mathbf{k}^2 and $T_{P\bar{Q} \rightarrow P\bar{Q}}(s_1)$ tends to $1/\log s_1$ or constant for $|s_1| \rightarrow \infty$. This, together with the factor $E_Q(\mathbf{k})$ in the denominator, gives rise to a quadratic divergence. For Σ_P^{tad} , eq.(2.6), one has the same type of divergence as $T_{P\bar{P} \rightarrow Q\bar{Q}}$ is evaluated at $s_1 = 0$ and is a constant.

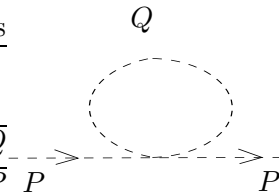


Figure 5: $\mathcal{O}(p^4)$ contribution of figs.2b and 4b. The loop is the only one appearing at $\mathcal{O}(p^4)$ CHPT.

A general coupled channel S-wave T-matrix from ref.[14], e.g. that involving $\pi\pi$, $K\bar{K}$ and $\eta\eta$ in $I=0$, has the structure,

$$T = [I + \mathcal{K} \cdot G]^{-1} \cdot \mathcal{K} , \quad (2.9)$$

with \mathcal{K} the interaction kernel that comprises the lowest order CHPT amplitudes plus the s-channel exchange of some scalar resonances, as told above, and G corresponds to the unitarity bubbles shown in fig.2. For more details see ref.[14]. The previous equation has the expansion,

$$T = [I - \mathcal{K} \cdot G + \mathcal{K} \cdot G \cdot \mathcal{K} + \dots] \cdot \mathcal{K} . \quad (2.10)$$

We notice that when $T = \mathcal{K}_2$ (the lowest order CHPT amplitudes), one has zero unitarity bubbles in fig.2b and fig.4b, and then both figures give the same diagram. This only happens for \mathcal{K}_2 at lowest order in CHPT, without the exchange of resonances, because for the latter the resonance propagators have different four-momentum and the diagrams are different. The local term \mathcal{K}_2 gives rise to the one loop diagram shown in fig.5, the only one that appears at next-to-leading order (NLO) in CHPT (at this order the rest of contributions come from local counterterms [2, 3]). In order to avoid this double-counting we then subtract the $\mathcal{O}(p^4)$ contribution to the integral in eq.(2.5), fig.2b. This is done explicitly below in eq.(2.33).

2.2 Regularization and renormalization

We now proceed with the evaluation of the integral in eq.(2.5) for Σ_P^U . The integral in eq.(2.6) for Σ_P^{tad} is a particular case of the previous evaluation since T_{ij} here is evaluated at $s_1 = 0$ and is just a constant. Firstly, we perform the angular integration and change to energy as integration variable.

$$\int \frac{d^3k}{(2\pi)^3 2E_Q(\mathbf{k})} T_{P\bar{Q} \rightarrow P\bar{Q}}(s_1) = \int_{M_Q}^{\infty} \frac{|\mathbf{k}| dE_Q}{4\pi^2} T_{P\bar{Q} \rightarrow P\bar{Q}}(s_1) . \quad (2.11)$$

We now introduce the new variable

$$t = M_Q/E_Q , \quad (2.12)$$

in terms of which the previous integral transforms in:

$$\frac{M_Q^2}{(2\pi)^2} \int_0^1 dt \frac{\sqrt{1-t^2}}{t^3} T_{P\bar{Q} \rightarrow P\bar{Q}}(s_1) , \quad (2.13)$$

with $s_1 = M_P^2 + M_Q^2 - 2M_P M_Q/t$. The integral above diverges quadratically for $t \rightarrow 0$. Then we take the integral,

$$\frac{M_Q^2}{(2\pi)^2} \int_{\varepsilon}^1 dt \frac{\sqrt{1-t^2}}{t^3} T_{P\bar{Q} \rightarrow P\bar{Q}}(s_1) , \quad (2.14)$$

with ε positive and small, taking at the end the limit $\varepsilon \rightarrow 0^+$. Notice that since $\varepsilon = M_Q/\Lambda$, with $\Lambda \gg M_Q$ the upper limit in the three-momentum of eq.(2.11), the previous limit is equivalent to $\Lambda \rightarrow +\infty$. In performing this limit we must identify those terms that scales as $1/\varepsilon^2$, $1/\varepsilon$ (equivalently as Λ^2 , Λ) and remove them from the result. In order to remove infinities one must work out algebraic expressions for the previous integral that explicitly show these diverging powers of ε . The problem of accomplishing this aim is the complicated matrix expression for the strong amplitude that prevents us from giving a close expression for the integral in eq.(2.14). However, we are only interested in isolating the dependence in ε and this can be done by performing a dispersion relation representation for $T_{P\bar{Q} \rightarrow P\bar{Q}}(s_1)$ in the physical Riemann sheet. In this way, the dependence on s_1 is given in simple terms, as we show below, allowing then to obtain the dependence on ε of the integral in eq.(2.14). The $T_{P\bar{Q} \rightarrow P\bar{Q}}(s_1)$ amplitude from ref.[14] has only one cut, the right or unitarity one, and tends to $1/\log s_1$ or constant when $s_1 \rightarrow \infty$. In order to perform the dispersion relation we take as integration contour a circle in the infinity deformed to engulf the real axis along the right hand cut , $s_{th} < s_1 < \infty$, with s_{th} the lightest meson-meson threshold with the $P\bar{Q}$ S-wave quantum numbers. We take one subtraction because of the aforementioned behaviour of $T_{ij}(s_1)$ ^{#4} at infinity. Then we have:

$$T_{ij}(s_1) = T_{ij}(s_2) + \frac{s_1 - s_2}{\pi} \int_{s_{th}}^{\infty} ds' \frac{\text{Im}T_{ij}(s')}{(s' - s_1)(s' - s_2)} + \sum_{\ell=1}^N \frac{(s_2 - s_1)R_{ij}^{(\ell)}}{(s_{\ell}^R - s_1)(s_{\ell}^R - s_2)} , \quad (2.15)$$

^{#4}We take now this shorter notation instead of the longer $T_{P\bar{Q} \rightarrow P\bar{Q}}(s_1)$. The subscripts i refer to the initial state and j to the final one

with s_2 the point where the subtraction has been performed. In addition, N is the number of poles of $T_{ij}(s)$ in the physical Riemann sheet and $R_{ij}^{(\ell)}$ is the residue of the ℓ_{th} pole at the position s_ℓ^R . Because of the Schwartz reflection principle any partial wave satisfies that $T_{ij}(s^*) = T_{ij}(s)^*$, so poles always appear as pairs in relative complex conjugate positions with complex conjugate residua. Taking then s_2 real in eq.(2.15) the contribution from the sum of poles is real for s_1 on the real s -axis.

A physical partial wave should not have any pole on the physical sheet with non-vanishing imaginary part. But notice that the lowest order CHPT S-wave amplitudes in I=1/2 ($K\pi \rightarrow K\pi$, $K\pi \rightarrow K\eta$ and $K\eta \rightarrow K\eta$) have each of them one pole at $s = 0$ due to the kinematical reason of having different masses, see ref.[14] for explicit expressions of those amplitudes. This pole at $s = 0$ for the interaction kernel drives the appearance of a pole in the final $K\pi \rightarrow K\pi$ S-wave typically at around $s = -0.25 \text{ GeV}^2$, not far away from its lowest order value. This poles gives rise to a non-negligible effect in the calculation of the π self-energy. There are also other poles with non-zero imaginary part. Reassuringly, these poles are always far away of the physical axis giving small and soft contributions to the real part of $T_{ij}(s_1)$ and are negligible for the calculation of self-energies. One also has to take into account that the amplitudes of ref.[14] can be improved by considering a more elaborated kernel by evaluating higher orders in the chiral expansion [50, 51, 52].

Let us proceed with the evaluation of the renormalized value of the divergent integral eq.(2.14) making use of the representation given in eq.(2.15) for the S-wave T-matrix elements. Both the contributions from the unitarity cut and poles involve the same kind integral,

$$J(s', s_2) = \int_\varepsilon^1 dt \frac{\sqrt{1-t^2}}{t^3} \frac{s_1(t) - s_2}{s' - s_1(t)}. \quad (2.16)$$

For the sum over the poles in eq.(2.15) the variable s' must be replaced by s_ℓ^R . For convenience, new variables a and b are introduced as follows,

$$a = \nu - \frac{s_2}{2M_P M_Q}, \quad b = \nu - \frac{s'}{2M_P M_Q}, \quad (2.17)$$

with $\nu = (M_P^2 + M_Q^2)/(2M_P M_Q)$. Notice that one can also write $1/t = \nu - s_1/2M_P M_Q$. Then,

$$J(s', s_2) = \int_\varepsilon^1 dt \frac{\sqrt{1-t^2}}{t^3} \frac{at - 1}{1 - bt} = - \int_\varepsilon^1 dt \frac{\sqrt{1-t^2}}{t^3} + (a - b) \int_\varepsilon^1 dt \frac{\sqrt{1-t^2}}{t^2} \frac{1}{1 - bt}. \quad (2.18)$$

The first integral is elementary, although its renormalized value requires some comments. The integral reads,

$$- \int_\varepsilon^1 dt \frac{\sqrt{1-t^2}}{t^3} = \frac{1}{2} \left\{ \frac{\sqrt{1-t^2}}{t^2} - \log \frac{1 + \sqrt{1-t^2}}{t} \right\}_\varepsilon^1 = -\frac{1}{2} \frac{\sqrt{1-\varepsilon^2}}{\varepsilon^2} + \frac{1}{2} \log \frac{1 + \sqrt{1-\varepsilon^2}}{\varepsilon}. \quad (2.19)$$

Now, when sending $\varepsilon \rightarrow 0^+$ both terms on the r.h.s. of the second equality diverge. Performing a power series around $\varepsilon = 0$ one has $-1/2\varepsilon^2 + (1 - 2 \log \varepsilon/2)/4 + \mathcal{O}(\varepsilon^2)$. The first term in this sum diverges like ε^{-2} and should be reabsorbed by appropriate chiral counterterms. The terms with positive powers of ε , not shown, vanish for $\varepsilon \rightarrow 0$ and the remaining contribution is,

$$\frac{1}{4} \left(1 - 2 \log \frac{M_Q}{2\Lambda} \right) = \frac{1}{4} \left(1 - 2 \log \frac{M_Q}{2\mu} \right) - \frac{1}{2} \log \frac{\mu}{\Lambda}. \quad (2.20)$$

The renormalization scale μ is introduced in the previous equation. In sending $\Lambda \rightarrow +\infty$ ($\varepsilon \rightarrow 0^+$), again the term $\log \mu/\Lambda$ diverges and should be reabsorbed in appropriate counterterms. Then one has:

$$- \int_0^1 dt \frac{\sqrt{1-t^2}}{t^3} \doteq \frac{1}{4} \left(1 - 2 \log \frac{M_Q}{2\mu} \right), \quad (2.21)$$

where the symbol \doteq , used for expressing our renormalized integrals, means equal up to terms divergent as ε^{-2} , ε^{-1} or $\log \varepsilon$, when $\varepsilon \rightarrow 0^+$. When giving our results we shall vary μ between 0.5 GeV and 1.2 GeV, taking care in this way of possible constants of order one that may change depending on the chosen renormalization scheme. E.g. the difference between our procedure and the results in the \overline{MS} scheme in dimensional regularization. This variation in μ will be a source of uncertainty in our results and it will be consider in the error analysis.

We now consider the other remaining integral in eq.(2.18). First let us assume that $|b| > 1$, which is equivalent from eq.(2.17) to $s' < (M_P - M_Q)^2$ or $s' > (M_P + M_Q)^2$, then:

$$\int_\varepsilon^1 dt \frac{\sqrt{1-t^2}}{t^2} \frac{1}{1-bt} = - \int_\varepsilon^1 dt \frac{\sqrt{1-t^2}}{t^2} \sum_{n=0}^K \frac{1}{(bt)^{n+1}} - \int_\varepsilon^1 dt \frac{\sqrt{1-t^2}}{t^2} \frac{1/(bt)^{K+2}}{1-1/bt}, \quad (2.22)$$

where we have made an expansion of $1/(1-1/bt)$ in powers of $1/bt$, keeping the remaining term. The finite contribution of the last term is suppressed by powers of $(1/b)^{K+1}$, together with a further suppression of the type $1/K$ from the $1/t^{K+4}$ factor in the integrand. In this way, the result is given as a sum in powers of $1/b$ (for $|b| > 1$) and convergence is reached typically for $K \gtrsim 10$. In our calculations we have kept K around 30 to have good numerical precision. The finite result kept from each term in the sum of the first integral in the previous equation is determined as previously discussed for eq.(2.21). We give in table 1 the calculation of the finite part of the integrals in eq.(2.22) for $n \leq 14$,

$$c_n \doteq - \int_0^1 dt \frac{\sqrt{1-t^2}}{t^{n+3}}, \quad n \geq 0. \quad (2.23)$$

The coefficients c_n for n odd are zero, simply because the expansion of $\sqrt{1-t^2}$ involves only even powers of t . We shall also present afterwards another method to calculate these integrals without involving any power expansion. We advance that both method coincide, which is a crossed check of our expressions and codes. We shall come back to this point below in this section.

c_n	Value	c_n	Value
c_0	$0.5966 - 0.5000 \log M_Q/\mu$	c_8	$0.0043 - 0.0273 \log M_Q/\mu$
c_2	$0.0554 - 0.1250 \log M_Q/\mu$	c_{10}	$0.0027 - 0.0205 \log M_Q/\mu$
c_4	$0.0173 - 0.0625 \log M_Q/\mu$	c_{12}	$0.0018 - 0.0161 \log M_Q/\mu$
c_6	$0.0079 - 0.0391 \log M_Q/\mu$	c_{14}	$0.0013 - 0.0131 \log M_Q/\mu$

Table 1: Values calculated for the coefficients c_n of eq.(2.23), $n \leq 14$. Coefficients with n odd are zero.

Hence, for $|b| > 1$,

$$J(a, b) \equiv J_+(a, b) = \frac{1}{4} \left(1 - 2 \log \frac{M_Q}{2\mu} \right) + (a - b) \sum_{n=0}^{\infty} \frac{c_{2n}}{b^{2n+1}}, \quad |b| > 1, \quad (2.24)$$

with $a(s_2)$ and $b(s')$ as arguments for the function J .

Let us now consider the case $|b| < 1$ in the calculation of the last integral of eq.(2.18) which occurs for $(M_P - M_Q)^2 < s' < (M_P + M_Q)^2$. Performing now the expansion in powers of b one has,

$$\int_{\varepsilon}^1 dt \frac{\sqrt{1-t^2}}{t^2} \frac{1}{1-bt} = \int_{\varepsilon}^1 dt \frac{\sqrt{1-t^2}}{t^2} \sum_{n=0}^K (bt)^n + \int_{\varepsilon}^1 dt \frac{\sqrt{1-t^2}}{t^2} \frac{(bt)^{K+1}}{1-bt} . \quad (2.25)$$

Again the finite contribution of the last integral in the previous equation is suppressed for large K and the sum converges for $K \gtrsim 10$. We now introduce the coefficients,

$$c'_n \doteq \int_0^1 dt t^{n-2} \sqrt{1-t^2} , \quad n \geq 0 , \quad (2.26)$$

and then for $|b| < 1$ one has,

$$J(a, b) \equiv J_-(a, b) = \frac{1}{4} \left(1 - 2 \log \frac{M_Q}{2\mu} \right) + (a-b) \sum_{n=0}^{\infty} c'_n b^n , \quad |b| < 1 . \quad (2.27)$$

Notice that c'_n is divergent only for $n = 0$ and 1, for $n \geq 2$ is an ordinary definite integral. In table 2 we show the coefficients c'_n for $n \leq 11$.

c'_n	Value	c'_n	Value
c'_0	-1.5708	c'_6	0.0982
c'_1	$-0.3069 - \log M_Q/\mu$	c'_7	0.0762
c'_2	0.7854	c'_8	0.0614
c'_3	0.3333	c'_9	0.0508
c'_4	0.1964	c'_{10}	0.0430
c'_5	0.1333	c'_{11}	0.0369

Table 2: Values calculated for the coefficients c'_n of eq.(2.26) for $n \leq 11$.

In terms of the results of eqs.(2.24) and (2.27) we are now in disposition to provide expressions for the integral of eq.(2.14). We split it in several parts corresponding to the dispersive integral, subtraction constant and poles.

The dispersive integral contributes as:

$$I_{disp}^{PQ} = \int_{\varepsilon}^1 dt \frac{\sqrt{1-t^3}}{t^3} \frac{s_1 - s_2}{\pi} \int_{sth}^{\infty} ds' \frac{\text{Im}T_{ij}(s')}{(s' - s(t))(s' - s_2)} \doteq$$

i) If $(M_P - M_Q)^2 > sth$

$$\frac{1}{\pi} \int_{sth}^{(M_P - M_Q)^2} ds' \frac{\text{Im}T_{ij}(s')}{(s' - s_2)} J_+(s', s_2) + \frac{1}{\pi} \int_{(M_P - M_Q)^2}^{(M_P + M_Q)^2} ds' \frac{\text{Im}T_{ij}(s')}{(s' - s_2)} J_-(s', s_2)$$

$$+ \frac{1}{\pi} \int_{(M_P + M_Q)^2}^{+\infty} ds' \frac{\text{Im}T_{ij}(s')}{(s' - s_2)} J_+(s', s_2)$$

ii) If $(M_P - M_Q)^2 < sth$

$$\frac{1}{\pi} \int_{sth}^{(M_P + M_Q)^2} ds' \frac{\text{Im}T_{ij}(s')}{(s' - s_2)} J_-(s', s_2) + \frac{1}{\pi} \int_{(M_P + M_Q)^2}^{+\infty} ds' \frac{\text{Im}T_{ij}(s')}{(s' - s_2)} J_+(s', s_2) \quad (2.28)$$

Notice that $(M_P + M_Q)^2 \geq s_{th}$. Let us remark that $J_+(s', s_2)$ vanishes like $-1/s'$ for $s' \rightarrow \infty$, as it is clear from eq.(2.24) taking into account that $c_0 = (1 - 2 \log M_Q/2\mu)/4$. This is why all the last integrals in the previous equations converge for $s' \rightarrow +\infty$.

The subtraction constant, $T_{ij}(s_2)$, in eq.(2.15), contributes as,

$$I_{subs}^{PQ} = T_{ij}(s_2) \int_{\varepsilon}^1 dt \frac{\sqrt{1-t^2}}{t^3} \doteq -T_{ij}(s_2) \frac{1}{4} \left(1 - 2 \log \frac{M_Q}{2\mu} \right), \quad (2.29)$$

from eq.(2.21).

The contribution of the sum of poles in eq.(2.15) is:

$$I_{pole}^{PQ} = - \sum_{\ell=1}^N \frac{R_{ij}^{(\ell)}}{(s_{\ell}^R - s_2)} J_+(a, b(s_{\ell}^R)), \quad (2.30)$$

because as told above the same integral eq.(2.16) also takes place in this case with $s' \rightarrow s_{\ell}^R$. We have only $J_+(a, b)$ since for this case always $|b| > 1$ as the poles happens far away in the complex plane or on the negative s -axis. The minus sign in front of eq.(2.30) appears because for each pole, according to eq.(2.15), one has $s_2 - s_1$ in the numerator while in the dispersion integral $s_1 - s_2$ occurs.

Thus, the contribution to the self-energy of the pseudoscalar P calculated from eq.(2.14) is given by the sum of eqs.(2.28), (2.29) and (2.30) times $M_Q^2/(2\pi)^2$. Of course, one must in addition sum each contribution for every pseudoscalar Q , according to eq.(2.5), giving rise to Σ_P^U .

One has still to remove from the previous sum its $\mathcal{O}(p^4)$ contribution to avoid double-counting with the tadpole contribution, as explained above after eq.(2.10). This is achieved by evaluating eq.(2.5) with $T_{P\bar{Q} \rightarrow P\bar{Q}}$ given by its $\mathcal{O}(p^2)$ expression. A general CHPT S-wave amplitude at $\mathcal{O}(p^2)$ has the form,

$$T_{ij}^{(2)}(s) = A + Bs + \frac{C}{s}. \quad (2.31)$$

The last term in the sum only appears for the $I=1/2$ $K\pi$ and $K\eta$ coupled channel amplitudes involving two particles with different masses. Then,

$$\begin{aligned} & \int_0^1 dt \frac{\sqrt{1-t^2}}{t^3} \left(A + Bs_1(t) + \frac{C}{s_1(t)} \right) \\ &= \int_0^1 \frac{\sqrt{1-t^2}}{t^3} (A + s_A B) - 2M_P M_Q B \int_0^1 dt \frac{\sqrt{1-t^2}}{t^4} + \frac{C}{s_A} \int_0^1 dt \frac{\sqrt{1-t^2}}{t^2} \frac{1}{t-f}, \end{aligned} \quad (2.32)$$

with $f = 1/\nu$ ($f < 1$ when $C \neq 0$) and $s_A = M_P^2 + M_Q^2$. The second integral in this equation vanishes according to the fact that the c_1 coefficient of eq.(2.23) is zero. The equation above can be rewritten conveniently as,

$$\begin{aligned} I_{rem}^{PQ} &= T_{ij}^{(2)}(s_A) \int_0^1 dt \frac{\sqrt{1-t^2}}{t^3} + \frac{C}{s_A} \int_0^1 dt \frac{\sqrt{1-t^2}}{t^3} \frac{f}{t-f} \\ &= -T_{ij}^{(2)}(s_A) \frac{1}{4} (1 - 2 \log \frac{M_Q}{2\mu}) - \frac{C}{s_A} \sum_{n=1} c_n f^n, \end{aligned} \quad (2.33)$$

with the coefficients c_n given in eq.(2.23).

The other contribution to Σ_P is Σ_P^{tad} , eq.(2.7). Its calculation, eq.(2.19), is straightforward and is completely analogous to the calculation of eq.(2.29). Then we have,

$$I_{tad}^{PQ} = \lambda_Q T_{ij}(0) \int_{\varepsilon}^1 dt \frac{\sqrt{1-t^2}}{t^3} \doteq -\lambda_Q \frac{T_{ij}(0)}{4} \left(1 - 2 \log \frac{M_Q}{2\mu} \right). \quad (2.34)$$

Hence, for eq.(2.7) one has:

$$\Sigma_P = - \sum_Q \frac{M_Q^2}{(2\pi)^2} \left(I_{subs}^{PQ} + I_{disp}^{PQ} + I_{pole}^{PQ} - I_{rem}^{PQ} \right) - \sum_{Q'} \frac{M_{Q'}^2}{(2\pi)^2} I_{tad}^{PQ'} \quad (2.35)$$

with $Q = \{\pi^0, \pi^+, \pi^-, K^0, \bar{K}^0, K^+, K^-, \eta\}$ and $Q' = \{\pi^0, \pi^+, K^+, K^0, \eta\}$. Notice that after the subtraction in eq.(2.29) of $\sum_Q I_{rem}^{PQ} M_Q^2 / (2\pi)^2$, the only contribution at $\mathcal{O}(p^4)$ of our result comes from $I_{tad}^{PQ} M_Q^2 / (2\pi)^2$ by substituting $T_{ij}(0)$ in eq.(2.34) by $T_{ij}^{(2)}(0)$, the corresponding lowest order CHPT amplitude. In this $\mathcal{O}(p^4)$ chase we have checked that $\sum_{Q'} I_{tad}^{PQ'} M_{Q'}^2 / (2\pi)^2$ reproduces the CHPT infrared logarithms on the quark masses in CHPT at $\mathcal{O}(p^4)$ [3].

The integral of eq.(2.16), $J(s', s_2)$, can also be integrated in terms of elementary functions, in numerical agreement with the results obtained from the series expansions.

$$\begin{aligned} J(s', s_2) &= - \int_{\varepsilon}^1 dt \frac{\sqrt{1-t^2}}{t^3} \frac{1-at}{1-bt} = - \int_{\varepsilon}^1 \frac{\sqrt{1-t^2}}{t^3} + (a-b) \int_{\varepsilon}^1 dt \frac{\sqrt{1-t^2}}{t^2} \\ &+ (a-b)b \int_{\varepsilon}^1 dt \frac{\sqrt{1-t^2}}{t} - (a-b)b \int_{\varepsilon}^1 dt \frac{\sqrt{1-t^2}}{t-1/b}. \end{aligned} \quad (2.36)$$

The first three integrals on the r.h.s of the second equality correspond to c_0 , c'_0 and c'_1 , respectively, that are already worked out. For the fourth integral,

$$\int dt \frac{\sqrt{1-t^2}}{t-c} = \sqrt{1-t^2} - c \arcsin t + (1-c^2) \int \frac{dt}{(t-c)\sqrt{1-t^2}}, \quad (2.37)$$

with $c = 1/b$. The last integral gives rise to,

$$\begin{aligned} \tilde{I} &= \int_{\varepsilon}^1 \frac{dt}{(t-1/b)\sqrt{1-t^2}} = \\ i) & \frac{1}{\sqrt{1-1/b^2}} \log \frac{1 + \sqrt{1-1/b^2}}{\varepsilon + 1/b}, \quad b > 1, \\ ii) & \frac{1}{\sqrt{1-1/b^2}} \log \frac{1 + \sqrt{1-1/b^2}}{\varepsilon - 1/b}, \quad b < -1, \\ iii) & \frac{-1}{\sqrt{1/b^2-1}} \left(\frac{\pi}{2} + \arcsin b \right), \quad 0 < b < 1, \\ iv) & \frac{1}{\sqrt{1/b^2-1}} \left(\frac{\pi}{2} + \arcsin b \right), \quad -1 < b < 0, \end{aligned} \quad (2.38)$$

Adding all the terms in eq.(2.36) one has:

$$J(s', s_2) = \frac{1}{4} + \frac{1}{2} \log \frac{2}{\varepsilon} + (a-b)b \log \frac{2}{\varepsilon} - (a-b)b(1-1/b^2) \tilde{I}. \quad (2.39)$$

In the expressions given for \tilde{I} with $|b| > 1$ in eq.(2.38), the first two lines, one has $\log(\varepsilon + 1/|b|) = \log \varepsilon + \log(1 + 1/\varepsilon|b|)$. This last term gives rise to an infinite series of divergent terms in powers of $1/(|b|\varepsilon)^n$ for $|b| > 1$ which are removed in the regularization process. Substituting also $\log \varepsilon$ by $\log M_Q/\mu$, introducing the renormalization scale μ , as we explained before, we end up with:

$$\begin{aligned}
& J(s', s_2) \doteq \\
i) \quad & J_+(a, b) = \frac{1}{4} + \frac{1}{2} \log \frac{2\mu}{M_Q} + (a-b)b \log 2 - (a-b)b(1 - \sqrt{1-1/b^2}) \log \frac{M_Q}{\mu} \\
& \quad - (a-b)b\sqrt{1-1/b^2} \log(1 + \sqrt{1-1/b^2}) , \quad |b| > 1 , \\
ii) \quad & J_-(a, b) = \frac{1}{4} + \frac{1}{2} \log \frac{2\mu}{M_Q} + (a-b)b \log \frac{2\mu}{M_Q} - (a-b)\sqrt{1-b^2} \left(\frac{\pi}{2} + \arcsin b \right) , \quad |b| < 1 .
\end{aligned} \tag{2.40}$$

These results agree numerically with the series of eq.(2.24) and (2.27), respectively, and can be used independently. In terms of these integrals one then evaluates all the contributions in eq.(2.35). Eq.(2.40) implies that for $|b| > 1$ then $J(a, b)$ cancels like $\propto a/b$ when $|b| \rightarrow \infty$. This is why, the integration over s' in I_{disp}^{PQ} , eq.(2.28), converges for $s' \rightarrow \infty$, as we have seen already in terms of the expansion eq.(2.24). Furthermore, this behaviour for $|b| \rightarrow \infty$ for $J(a, b)$ is also interesting in the sense that if we take s_2 such that $a = 0$ then $J(a, b)$ will vanish like $\mathcal{O}(b^{-2})$ for $b \rightarrow \infty$. One can take advantage of this fact since the pole contributions will tend to vanish because poles typically appear with large values of s_ℓ^R and then with $|b|$ large. Thus, we fix $s_2 = s_A = M_P^2 + M_Q^2$ in the following which, from eq.(2.17), implies that $a = 0$. This choice also makes that all contributions in eq.(2.35) have natural size.

We shall often remove the $\mathcal{O}(p^4)$ contribution to Σ_P and then write Σ_P^H for its contributions of $\mathcal{O}(p^6)$ and higher. As mentioned, this is obtained by the replacement $T_{ij}(0) \rightarrow T_{ij}(0) - T_{ij}^{(2)}(0)$ in eq.(2.34) for the tadpole contribution. Once the $\mathcal{O}(p^4)$ contribution is removed we add to Σ_P^H the $\mathcal{O}(p^4)$ CHPT contribution from ref.[3],

$$\begin{aligned}
M_\pi^2 &= \overset{\circ}{M}_\pi^2 \left\{ 1 + \mu_\pi - \frac{1}{3}\mu_\eta + 2\hat{m}K_3 + K_4 \right\} , \\
M_K^2 &= \overset{\circ}{M}_K^2 \left\{ 1 + \frac{2}{3}\mu_\eta + (\hat{m} + m_s)K_3 + K_4 \right\} , \\
M_\eta^2 &= \overset{\circ}{M}_\eta^2 \left\{ 1 + 2\mu_K - \frac{4}{3}\mu_\eta + \frac{2}{3}(\hat{m} + m_s)K_3 + K_4 \right\} + \overset{\circ}{M}_\pi^2 \left\{ -\mu_\pi + \frac{2}{3}\mu_K + \frac{1}{3}\mu_\eta \right\} + K_5 ,
\end{aligned} \tag{2.41}$$

where,

$$\begin{aligned}
K_3 &= \frac{8B_0}{F_0^2}(2L_8^r - L_5^r) , \quad K_4 = (2\hat{m} + m_s)\frac{16B_0}{F_0^2}(2L_6^r - L_4^r) , \\
K_5 &= (m_s - \hat{m})^2 \frac{128}{9} \frac{B_0^2}{F_0^2}(3L_7 + L_8^r) , \quad \mu_Q = \frac{1}{32\pi^2} \frac{\overset{\circ}{M}_P}{F_0^2} \log \frac{\overset{\circ}{M}_P}{\mu^2} .
\end{aligned} \tag{2.42}$$

The symbol $\overset{\circ}{M}_P$ denotes the bare mass of the pseudoscalar P corresponding to the lowest order CHPT result,

$$\overset{\circ}{M}_\pi^2 = 2B_0\hat{m} , \quad \overset{\circ}{M}_K^2 = B_0(\hat{m} + m_s) , \quad \overset{\circ}{M}_\eta^2 = \frac{2}{3}B_0(\hat{m} + 2m_s) , \tag{2.43}$$

and B_0 measures the strength of the quark condensate $\langle 0|\bar{q}q|0\rangle = -F_0^2 B_0 + \mathcal{O}(m_q^2)$ in the SU(3) chiral limit. We will denote the $\mathcal{O}(p^4)$ CHPT self-energies by $\Sigma_P^{4X} = M_P^2 - \overset{\circ}{M}_P^2$, eq.(2.41). Notice that from eq.(2.43) $\overset{\circ}{M}_\eta^2$ always satisfies the Gell-Mann-Okubo mass relation,

$$\overset{\circ}{M}_\eta^2 = \frac{1}{3}(4 \overset{\circ}{M}_K^2 - \overset{\circ}{M}_\pi^2) . \quad (2.44)$$

On the other hand, the L_i^r coefficients are the renormalized values of the low energy CHPT counterterms at $\mathcal{O}(p^4)$ from ref.[3].

The mass equation one has to solve is,

$$M_P^2 = \overset{\circ}{M}_P^2 + \Sigma_P(\overset{\circ}{M}_Q^2; M_Q^2) , \quad (2.45)$$

with Σ_P given in eq.(2.35). The dependence on the bare masses $\overset{\circ}{M}_Q^2$ originates from the dependence on the explicit inclusion of the quark mass matrix in CHPT from where the interaction kernel \mathcal{K} is calculated [14].

Once we subtract from Σ_P the $\mathcal{O}(p^4)$ contribution and add then the pure CHPT result, eq.(2.41), we have then the equations,

$$M_P^2 = \overset{\circ}{M}_P^2 + \Sigma_P^{4X}(\overset{\circ}{M}_Q^2; L_i^r) + \Sigma_P^H(\overset{\circ}{M}_Q^2; M_Q^2) \quad (2.46)$$

that reproduces the CHPT self-energies up to $\mathcal{O}(p^4)$ and resums the higher order contributions from the diagrams of figs.2 and 4

Our analysis is performed in the isospin limit, $m_u = m_d = \hat{m}$ and then M_P^2 above refers to the masses of the lightest pseudoscalars in the isospin limit. To determine these masses we employ the Dashen theorem [53] which states that at the lowest nontrivial order in e^2 the neutral particles π^0 and K^0 do not receive electromagnetic contributions, while these are the same for $M_{\pi^+}^2$ and $M_{K^+}^2$. In this way,

$$M_\pi^2 = M_{\pi^0}^2 \simeq (135 \text{ MeV})^2 , \quad M_K^2 = (M_{K^+} + M_{K^0}^2 - M_{\pi^+}^2 + M_{\pi^0}^2)/2 \simeq (495 \text{ MeV})^2 , \quad (2.47)$$

are taken as the pion and kaon masses in the isospin limit, respectively. Violations of the previous relation for the pion mass are expected to be tiny, $\mathcal{O}((m_u - m_d)^2)$ [3], from the pure QCD side, and $\mathcal{O}(e^2 m_\pi^2 / (8\pi^2 f_\pi^2))$ from electromagnetic interactions for the π^0 mass. More substantial seems to be the violations of the Dashen theorem, of order $e^2 M_K^2$ [54, 55, 56]. So that, if we write $M_K^2 = [M_{K^+}^2 + M_{K^0}^2 - (1 + \delta D)(M_{\pi^+}^2 - M_{\pi^0}^2)] / 2$, with δD measuring the deviation with respect to the Dashen theorem, then as a conservative estimate, δD is expected to be in the range $0 - 2$ [18] from refs.[55, 56]. But even so, the changes in M_K^2 are at most a 0.5%, which can be discarded within the definitely larger uncertainties of our calculations, to be shown in the next sections.

3 Dynamical self-energies

We first consider the results from eq.(2.45) solving for $\overset{\circ}{M}_{\pi,K}^2$ (equivalently for $B_0 \hat{m}$ and $B_0 m_s$, see eq.(2.43)) and for M_η^2 . In this section the η is actually the η_8 since we are not including any source of $\eta - \eta'$ mixing. The distinction between the η and η_8 is accomplished in the next section when matching with CHPT to $\mathcal{O}(p^4)$ through the L_7 counterterm [3]. Having made this point clear, along this section we will however still denominate the η_8 mass by M_η , unless the symbol M_{η_8} is explicitly used.

In perturbative studies one solves iteratively eq.(2.45). In this way, for the first round, we will use physical masses in all the arguments of the self-energies $\Sigma_P(\overset{\circ}{M}_Q^2; M_Q^2)$. Then, we have the equations,

$$\overset{\circ}{M}_P^2 = M_P^2 - \Sigma_P(M_Q^2; M_Q^2), \quad (3.48)$$

with the resulting values (in MeV):

$$\overset{\circ}{M}_\pi = 108 \pm 4, \quad \overset{\circ}{M}_K = 422 \pm 18, \quad M_\eta = 660 \pm 17. \quad (3.49)$$

The errors are calculated by performing a Monte-Carlo sampling of the free parameters of the T-matrix of ref.[14], within the errors there given,^{#5} and the renormalization scale μ introduced above in the evaluation of the self-energies, eq.(2.19), between 0.5 and 1.2 GeV. This will be the standard procedure to evaluate errors in our work and should be understood in the following.

Performing one more iteration in eq.(2.45), i.e. using the previous bare masses in the appropriate arguments of the self-energies, it results

$$\overset{\circ}{M}_\pi = 158 \pm 7, \quad \overset{\circ}{M}_K = 511 \pm 12, \quad M_\eta = 627 \pm 15. \quad (3.50)$$

We observe significant differences between eqs.(3.49) and (3.50) for $\overset{\circ}{M}_\pi^2$ and $\overset{\circ}{M}_K^2$, which is a clear indication that higher orders corrections, of $\mathcal{O}(p^6)$ and superior, are relevant for the calculation of the lightest pseudoscalar self-energies in SU(3), as shown in ref.[57], where the masses were calculated at $\mathcal{O}(p^6)$ in CHPT.

Because of the large variation between the values in eqs.(3.49) and (3.50), the eqs.(2.45) should be solved exactly. A first method for solving them is by iteration and after i iterations the approximated solution is given by,

$$\begin{aligned} \overset{\circ}{M}_{\pi;i}^2 &= M_\pi^2 - \Sigma_\pi(\overset{\circ}{M}_{Q;i-1}^2; M_\pi^2, M_K^2, M_{\eta;i-1}^2), \\ \overset{\circ}{M}_{K;i}^2 &= M_K^2 - \Sigma_K(\overset{\circ}{M}_{Q;i-1}^2; M_\pi^2, M_K^2, M_{\eta;i-1}^2), \\ M_{\eta;i}^2 &= \overset{\circ}{M}_{\eta;i-1}^2 + \Sigma_\eta(\overset{\circ}{M}_{Q;i-1}^2; M_\pi^2, M_K^2, M_{\eta;i-1}^2). \end{aligned} \quad (3.51)$$

The symbol $\overset{\circ}{M}_{Q;i}$ refers to the value of the bare mass of the pseudoscalar Q for the i_{th} iteration. The bare mass $\overset{\circ}{M}_{\eta;i}^2$ always satisfy the Gell-Mann-Okubo mass relation, eq.(2.44), in terms of $\overset{\circ}{M}_{\pi;i}^2$ and $\overset{\circ}{M}_{K;i}^2$. Since we are now varying the bare masses employed in the kernels for the T-matrices we refit the data for every value of the given bare masses. Then the T-matrix changes as a function of the values employed in each step. However, we observe that the values of the free parameters of the kernel [14] change within the error band given to them and, hence, this refitting process is indeed accounted for by the error analysis. Another technicality, that only applies in this section where we distinguish between M_η and M_{η_8} masses, is in order. When solving and/or iterating eq.(2.45) for M_η^2 , we will always keep for the evaluation of the S-waves the physical mass of the η meson in the calculation of the $G_{\eta\pi}$, $G_{K\eta}$ and $G_{\eta\eta}$ functions in eq.(2.9). This is done because the physical data, shown in fig.1, are sensible to the physical thresholds involving the η meson (like $\eta\pi$ with I=1, $K\eta$ in I=1/2 or $\eta\eta$ in I=0). Otherwise we cannot fit the experiment. Let us recall that the G_i functions are the responsible for unitarity and the right position of physical cuts.

^{#5}We have made a new fit, including some more recent data, and the resulting fit has central values for the free parameters that are compatible with those of ref.[14], within the shown errors in this reference.

We also solve eq.(2.45) in another way having then two independent numerical methods to compare with. It consists of minimizing the function,

$$\begin{aligned}
S(\overset{\circ}{M}_\pi, \overset{\circ}{M}_K) &= \left(\frac{\overset{\circ}{M}_\pi + \Sigma_\pi(\overset{\circ}{M}_Q; M_Q^2)}{M_\pi^2} - 1 \right)^2 + \left(\frac{\overset{\circ}{M}_K + \Sigma_K(\overset{\circ}{M}_Q; M_Q^2)}{M_K^2} - 1 \right)^2 \\
&+ \left(\frac{\overset{\circ}{M}_\eta + \Sigma_\eta(\overset{\circ}{M}_Q; M_Q^2) - M_\eta^2}{M_K^2} \right)^2 .
\end{aligned} \tag{3.52}$$

This method is more robust than the iterative one, since it can provide solutions where the former does not converge, as we show explicitly below when we discuss cases from eq.(2.46). In our present case both methods give the same values (in MeV),

$$\overset{\circ}{M}_\pi = 126 \pm 4 , \quad \overset{\circ}{M}_K = 476 \pm 10 , \quad M_\eta = 635 \pm 15 . \tag{3.53}$$

One observes significant variations between the exact result and the first and second iterated solutions, eq.(3.49) and (3.50), respectively. It is then worth stressing the importance of solving eqs.(2.45) exactly.

Regarding the sizes of the self-energies, we have,

$$\frac{\Sigma_P(\overset{\circ}{M}_Q; M_Q^2)}{M_P^2} = 0.11 \pm 0.06 , \quad 0.08 \pm 0.04 , \quad 0.26 \pm 0.06 , \tag{3.54}$$

for pions, kaons and etas, respectively. We then observe that most of the physical masses of the pseudoscalars is due to the bare mass and that the dynamical contributions because of their self-interactions are rather small for pions and kaons, although more significant for the η_8 ($\overset{\circ}{M}_\eta = 545$ MeV from the Gell-Mann-Okubo relation, eq.(2.44), and the pion and kaon bare masses of eq.(3.53)). We then favour the standard CHPT scenario, where the linear quark mass term is assumed to dominate the pseudoscalar masses, versus the generalized one [58]. The M_{η_8} that we obtain, around 635 MeV, is larger than the one of the η physical meson, 547.45 MeV, that is very close to the bare η mass calculated from Gell-Mann-Okubo. Our value for M_{η_8} is very similar to that of ref.[59], $M_{\eta_8} = 639$ MeV, obtained by saturating the $\mathcal{O}(p^4)$ CHPT counterterms from the tree-level exchange of explicit scalar resonance fields. However, since the first scalar nonet of the lightest resonances is dominantly from dynamical origin we consider our approach more reliable since this is the way in which the lightest scalar resonances are realized in nature.

We also show our results for the solution of eq.(2.45) using the parameters in the S-waves with their values determined by fitting experimental data employing always physical masses in the interaction kernel. That is, we do not refit them in terms of the bare masses, as done to calculate the previous numbers eq.(3.53). Differences would be of higher order in the kernels. The resulting numbers are in fact very similar to those already determined,

$$\overset{\circ}{M}_\pi = 125 \pm 4 , \quad \overset{\circ}{M}_K = 477 \pm 10 , \quad M_\eta = 633 \pm 15 . \tag{3.55}$$

Thus, the process of refitting the free parameters in the S-waves by distinguishing between physical and bare masses, where it corresponds, just introduces minor corrections (compared with the quoted errors) and will not be further considered in the subsequent.

	First set ref.[57]	Second set ref.[60]	Third set ref.[61]
L_4^r	0	0.22 ± 30	-0.3 ± 0.5
L_5^r	0.97 ± 0.11	-	1.4 ± 0.5
L_6^r	0	-	-0.2 ± 0.3
L_7^r	-0.31 ± 0.14	-	-0.4 ± 0.2
L_8^r	0.60 ± 0.18	-	0.9 ± 0.3
$2L_6^r - L_4^r$	0	-0.22 ± 0.30	-0.1 ± 0.8
$2L_8^r - L_5^r$	0.23 ± 0.38	-	0.4 ± 0.8
$3L_7^r + L_8^r$	-0.33 ± 0.46	-	-0.3 ± 0.7

Table 3: Typical values for $L_i^r(M_\rho) \times 10^3 \mathcal{O}(p^4)$ χ PT counterterms. For the value of $2L_6^r - L_4^r$ given in the second set it has been assumed that $L_6^r = 0$, as in the first and third sets.

Taking into account the expression for the bare masses in terms of the quark masses, eq.(2.43), and the values of the former ones in eq.(3.53), one has,

$$r_m = \frac{m_s}{\hat{m}} = 2 \frac{\overset{\circ}{M}_K^2}{\overset{\circ}{M}_\pi^2} - 1 = 27.1 \pm 2.5 . \quad (3.56)$$

This value has not involved any new free parameters once the strong T-matrices have been given. This number, within errors, is in the bulk of other determinations, $r_m = 25.7 \pm 2.6$ from $\mathcal{O}(p^4)$ CHPT [3], or with the more refined one of ref.[21], $r_m = 24.4 \pm 1.5$, and also with lattice determinations [18], 27.4 ± 0.5 .

4 Including $\mathcal{O}(p^4)$ CHPT self-energies

In this section we include the CHPT self-energies at $\mathcal{O}(p^4)$ and correct them by adding Σ_P^H , defined just before eq.(2.41), resumming in this way the effects of higher orders corrections ($\mathcal{O}(p^6)$ and higher). Because in this section we include the CHPT self-energies up to $\mathcal{O}(p^4)$, the $\eta - \eta'$ mixing is then incorporated at this order by the counterterm L_7 and M_η is fixed to its physical value [3]. Eq.(2.46) incorporates the combinations of the low energy constants $L_{(5,8)} \equiv 2L_8^r - L_5^r$, $L_{(4,6)} \equiv 2L_6^r - L_4^r$ and $L_{(7,8)} \equiv 3L_7^r + L_8^r$, as explicitly shown in eqs.(2.41) and (2.42). In table 3 we show typical values for these $\mathcal{O}(p^4)$ LECs from ref.[57], which includes in its fits the $\mathcal{O}(p^6)$ CHPT amplitudes, another value for L_4^r [60], as well as the values from the $\mathcal{O}(p^4)$ study of ref.[61]. All the LECs shown in the present work are given for a renormalization scale equal to M_ρ . In this table, it should be understood that when the value for a given L_i^r is not shown then it is the same as for the first set [57]. We also show explicitly for each set the values of $L_{(4,6)}$, $L_{(5,8)}$ and $L_{(7,8)}$.

As a function of $L_{(4,6)}$ and $L_{(5,8)}$, we solve first for the $\overset{\circ}{M}_\pi^2$ and $\overset{\circ}{M}_K^2$ bare masses in eqs.(2.46),

$$\begin{aligned} \overset{\circ}{M}_\pi^2 &= M_\pi^2 - \Sigma_\pi^{4\chi}(\overset{\circ}{M}_Q^2) - \Sigma_\pi^H(\overset{\circ}{M}_Q^2; M_Q^2) \\ \overset{\circ}{M}_K^2 &= M_K^2 - \Sigma_K^{4\chi}(\overset{\circ}{M}_Q^2) - \Sigma_K^H(\overset{\circ}{M}_Q^2; M_Q^2) . \end{aligned} \quad (4.57)$$

Once we calculate $\overset{\circ}{M}_\pi^2$ and $\overset{\circ}{M}_K^2$ from the previous equations we fix $\overset{\circ}{M}_\eta^2$ using the Gell-Mann-Okubo

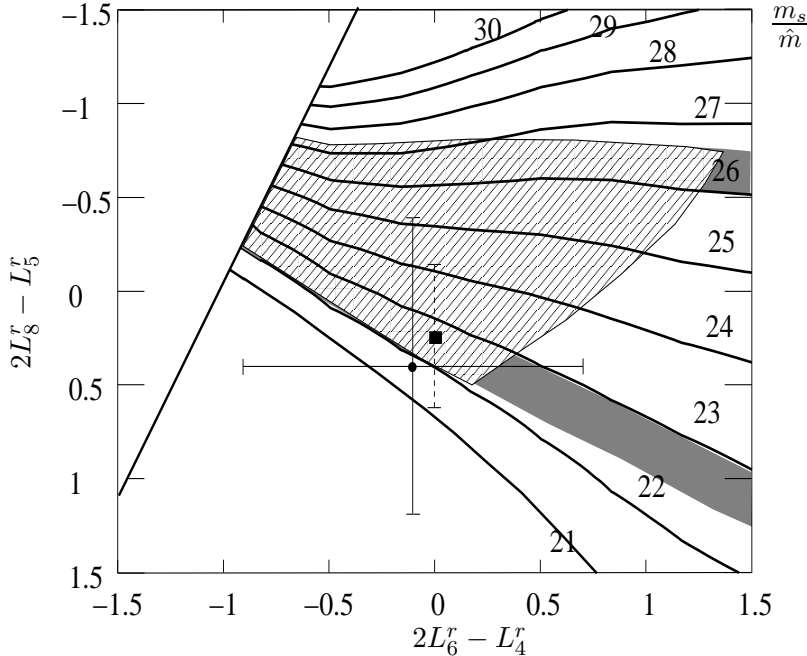


Figure 6: Contour-plot for $r_m = m_s/\hat{m}$ as a function of $L_{(4,6)}$ and $L_{(5,8)}$. The circle corresponds to the third set and the square to the first one in table 3. For more details see the text.

relation, eq.(2.44), and from the equation,

$$M_\eta^2 = \overset{\circ}{M}_\eta^2 + \Sigma_\eta^{4\chi}(\overset{\circ}{M}_Q^2) + \Sigma_\eta^H(\overset{\circ}{M}_Q^2; M_Q^2), \quad (4.58)$$

we then solve for $L_{(7,8)}$.

Eq.(4.57) is solved simultaneously by the iterative and fit methods, as discussed in the previous section.^{#6} Both methods agree when the former converges but, as told above, the fit method is able to provide solutions to eq.(4.57) even when the iterative one does not converge. This occurs in our present case due to the large variation allowed in the values explored for the L_i^r .

In fig.6 we show by contour-plot lines the calculated values for $r_m = m_s/\hat{m}$ as a function of $L_{(4,6)}$ and $L_{(5,8)}$.^{#7} The up-left corner where no contour lines are plotted determines a region where no solutions of eq. (4.57) are found. The range of values for $2L_6^r - L_4^r$ and $2L_8^r - L_5^r$ has been chosen to span generously the values of table 3 within errors. If one takes into account the value of m_s/\hat{m} from CHPT [21], 24.4 ± 1.5 , the preferred region of $2L_6^r - L_4^r$ and $2L_8^r - L_5^r$ would be about in between the 23 and 26 contour lines. The shadowed areas below and above these lines represent the uncertainties of our calculation in these lines due to the variation in the renormalization scale, $\mu \sim [0.5, 1.2]$ GeV, and in the input parameters for the S-waves. Hence, they delimit the allowed bounded region of $2L_6^r - L_4^r$ and $2L_8^r - L_5^r$ that is permitted if the result $m_s/\hat{m} = 24.4 \pm 1.5$ [21] is taken. The same kind of considerations could be done for any other value taken for m_s/\hat{m} . The stripped region will be explained below.

It is worth comparing the result in fig.6 with the calculation obtained by considering the self-energies only up to the $\mathcal{O}(p^4)$ CHPT. The latter calculation is shown in fig.7. The difference is typically about

^{#6}The last term on the r.h.s. of eq.(3.52) is removed since we are now considering the solution for $\overset{\circ}{M}_\pi$ and $\overset{\circ}{M}_K$ only.

^{#7}In the whole manuscript, the values of the LECs displayed are given in units of 10^{-3} .

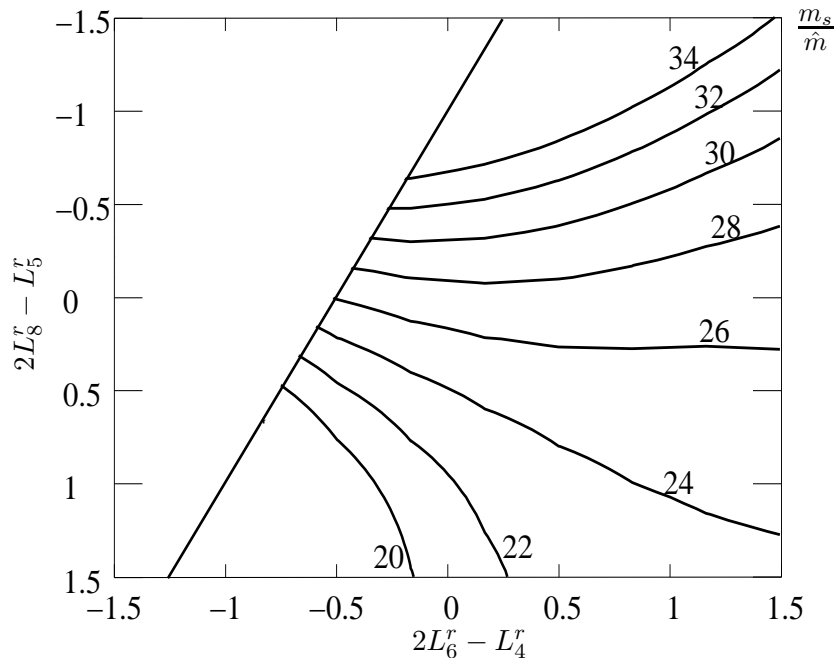


Figure 7: Contour-plot for $r_m = m_s/\hat{m}$ as a function of $L_{(4,6)}$ and $L_{(5,8)}$ obtained by employing only the $\mathcal{O}(p^4)$ CHPT self-energies.

2-3 units between both calculations. This makes manifest the important role of the orders higher than fourth one.

In fig.8, within the same range for $L_{(5,8)}$ and $L_{(4,6)}$ as in fig.6, we show by contour plots the values for $L_{(7,8)}$ resulting of solving eq.(4.58). In an analogous way to the m_s/\hat{m} case, one can delimit a region of allowed combination of LECs by providing some numerical input for $L_{(7,8)}$. If one considers the value of $L_{(7,8)} = -0.33 \pm 0.46$ [57] at $\mathcal{O}(p^6)$, and $L_{(7,8)} = -0.3 \pm 0.7$ [61] at $\mathcal{O}(p^4)$, the preferred $L_{(5,8)}$, $L_{(4,6)}$ region would be roughly in the interval $[-1, 0.4]$. Again the shadowed area along these lines represents the uncertainties of our calculation in these lines.

The stripped area in figs.6 and 8 represents the overlap between the allowed regions of both figures. In the next section we will restrict further this region by invoking lattice QCD.

5 Including lattice QCD

In order to obtain a sharper determination for the self-energies and quark mass ratio r_m , we employ our eq.(2.46) to reproduce the quark mass dependence of the recent lattice determinations of pseudoscalar masses from the MILC Collaboration [17] with three dynamical quarks, u , d and s . These determinations are nowadays performed for higher values of the masses of the lightest quarks, u and d , and parameterizations are needed to bring them down to physical values and determine m_u , m_d and m_s [18, 19]. We must say that we do not consider effects from the finite lattice volume and finite lattice spacing. Our aim here is just to have more points with which to compare, including those for unphysical values of quark masses and not only the physical ones, so that we can obtain a more constraint determination for $L_{(5,8)}$ and $L_{(4,6)}$. Indeed, we believe that the other sources of errors in our calculations are by far much larger than those lattice artifacts.

The strategy is the following. The MILC Collaboration [17] provides pseudoscalar meson masses as a

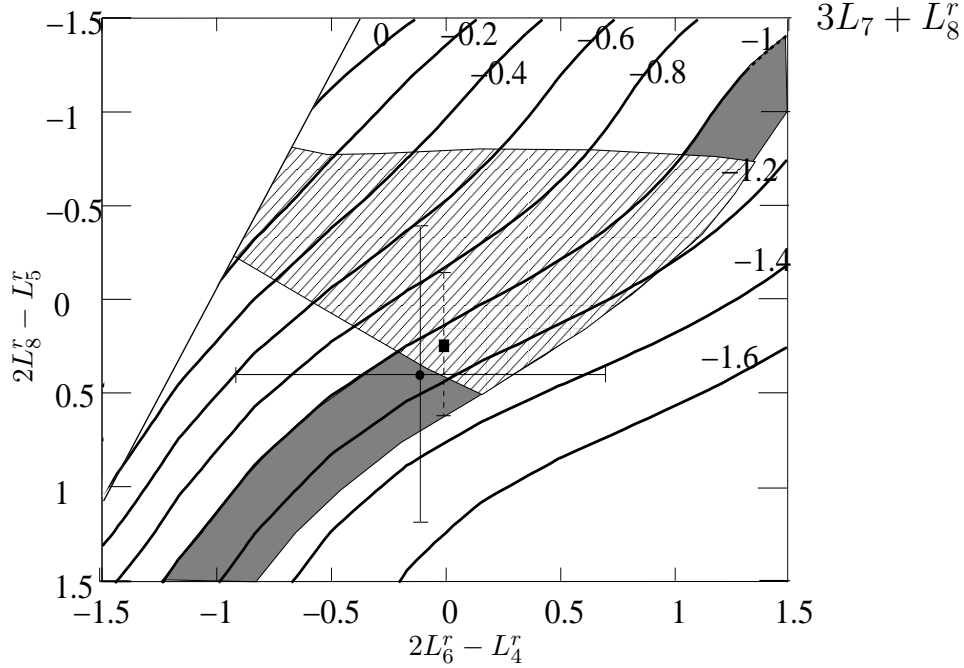


Figure 8: Contour-plot for $L_{(7,8)}$ as a function of $L_{(4,6)}$ and $L_{(5,8)}$. For the meaning of the points see fig.6.

function of the quark ones, measured in terms of the lattice spacing a , which is known with an error of about 1.2%. Current quark masses and those of lattice are proportional [18], so we write the bare meson masses in eq.(2.43) in terms of the lattice quark masses as,

$$\overset{\circ}{M}_\pi^2 = 2B_0C(a)a\hat{m} , \quad \overset{\circ}{M}_K^2 = B_0C(a)a(\hat{m} + m_s) , \quad \overset{\circ}{M}_\eta^2 = \frac{2}{3}B_0C(a)a(\hat{m} + 2m_s) , \quad (5.59)$$

and treat $B_0C(a)$ as a free parameter in our fits to the three flavour runs of ref.[17]. Notice that the constant $C(a)$ depends on the the lattice spacing a and its dependence can be found in ref.[19] at the two loop level. Previous calculations at the one loop level [18] gave a value for $m_s^{\overline{MS}}(2\text{GeV}) = 76 \pm 8$ MeV, to be compared with the latest value given in ref.[19] $m_s^{\overline{MS}}(2\text{GeV}) = 87 \pm 6$ MeV. This substantial shift comes from the improvement in the determination of $C(a)$ and we use the two loop result of ref.[19]. Ref.[17] gives the so called “coarse” lattice runs with $a_{coarse} \simeq 0.12$ fm, and the “fine” lattices with $a_{fine} \simeq 0.09$ fm. Making use of ref.[19] we then determine that,

$$C(a_{fine})/C(a_{coarse}) = 2.76/1.85 = 1.49 , \quad (5.60)$$

for $\mu = 2$ GeV. From this relation we fix $C(a_{fine})$ in terms of $C(a_{coarse})$ and take the latter as free parameter, which will be referred in the following just as C . At this point we take advantage of the fact that the constant C does not depend on the value of the quark mass in very good numerical accuracy (at the level of 0.1% [18, 19]) and we use the same value for all the lattice runs. We solve eq.(2.46) for the kaon and pion masses given by lattice QCD in terms of the quark masses used in the corresponding run by the MILC Collaboration [17]. For the lattice M_K^2 and M_π^2 points the only free parameters are B_0C , $L_{(4,6)}$ and $L_{(5,8)}$, while for M_K^2 and M_π^2 at the physical limit we have in addition $\overset{\circ}{M}_\pi^2$ and $\overset{\circ}{M}_K^2$. But from the mass equations for the physical points one can obtain $L_{(4,6)}$ and $L_{(5,8)}$ as a function of $\overset{\circ}{M}_\pi^2$

and M_K and hence the only free parameters in the fit to lattice data are B_0C , M_π and M_K . In the fit we do not consider the two points of the fine lattice run with $\hat{m}/m_s = 0.0124/0.031 = 2.5$ because it implies a rather heavy pion with a mass of 470 MeV [17]. This would require refit the parameters of our T-matrix to this lattice world of heavy pions. Of course, this refit cannot be performed because the data on inelasticities and phase shifts are not provided in ref.[17]. We then restrict ourselves to the case of lighter pions with $m_s/\hat{m} \leq 5$.

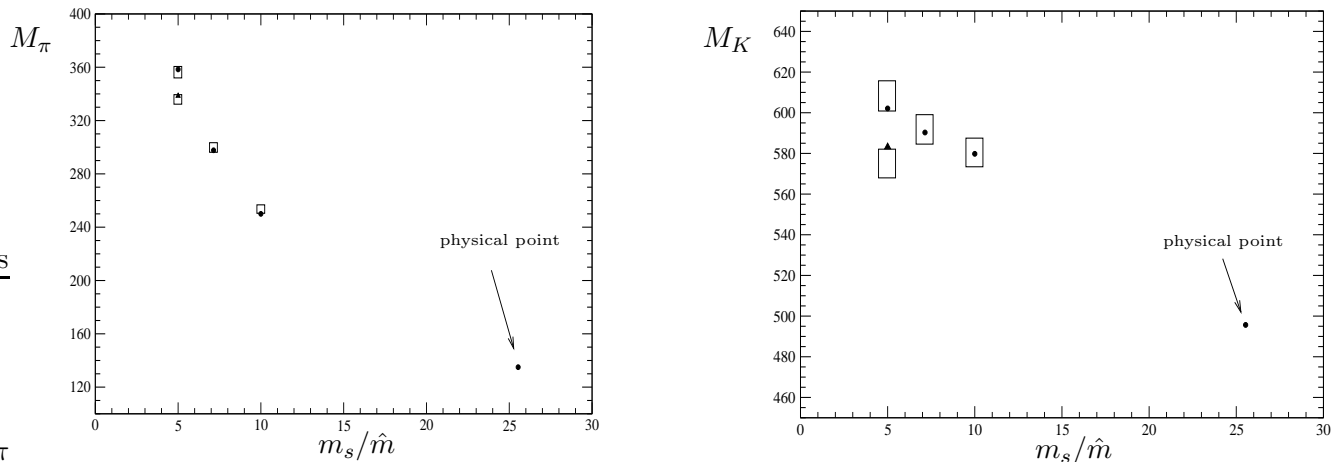


Figure 9: Lattice data from the MILC Collaboration [17] and their reproduction by our parameterization. The masses are given in MeV. The size of the squares corresponds to a relative error of 1.2%, the one given to a in ref.[17]. The circles refer to our calculations for the coarse lattices and the triangles for the fine ones. The physical mass values are signaled out by an arrow.

In fig.9a, b we show the reproduction of the lattice points [17] and of the physical values for the pion and kaon masses, respectively. The size of the squares corresponds to a relative error of 1.2%, the one given to a [17]. The circles correspond to our points for the coarse lattices and the triangles for the fine lattice runs. The arrows indicate the values of the physical kaon and pion masses. We reproduce very well the lattice data, despite the very small error, of about 1%. It is also worth stressing at this point that we also reproduce simultaneously all the scattering data given in fig.1.

From this fit we get the values,

$$2L_8^r - L_5^r = -0.52 \pm 0.43 \quad , \quad 2L_6^r - L_4^r = -0.20 \pm 0.17 \quad , \quad (5.61)$$

where, as usual, the errors come from the variation of μ and the parameters of the S-waves from ref.[14] within a Monte Carlo code. In fig.10, over the same plot as in fig.6, we show by the solid ellipse the one sigma region for $L_{(4,6)}$ and $L_{(5,8)}$. We also see in this figure that this region is well inside the favoured one determined in section 4 and denoted by the stripped area.

These values can be compared with the results of the works shown in table 3 and with the result from the MILC collaboration [62] $2L_8^r - L_5^r = 0.16 \pm 0.2$, $2L_6^r - L_4^r = 0.4 \pm 0.4$, given by the solid point in fig.10. We agree with both combinations of LECs at the level of one σ , although our numbers are on the lower side.

The corresponding ratio of quark masses is then,

$$\frac{m_s}{\hat{m}} = 25.6 \pm 2.5 \quad . \quad (5.62)$$

This value is in perfect agreement with 24.4 ± 1.5 from ref.[21]. Even at the level of the central values the difference between them is smaller than the error bars from both determinations. The previous result is also in agreement, at the level of one sigma, with the value 27.4 ± 0.5 determined in ref.[18] by taking down to the physical values of the lightest quark masses the lattice results on the pseudoscalar masses from the MILC Collaboration with Staggered CHPT. However, the difference between the central values of r_m of eq.(5.62) and ref.[18] is rather large, 2 units, particularly when compared with the error of 0.5 from ref.[18]. At this point, it is worth stressing that we have been able to give, with a non-perturbative chiral parameterization, a remarkably good reproduction of the lattice data, see fig.9, while giving rise a value for r_m significantly smaller than that of ref.[18] and in the range of values previously predicted from CHPT and phenomenology [21]. Thus, we certainly can conclude that it is not a *necessary* feature of the lattice runs of pseudoscalar masses by the MILC Collaboration [18] having a significantly larger m_s/\hat{m} value than that previously determined in ref.[21].

With respect to the bare masses one has,

$$\overset{\circ}{M}_\pi^2 = 125.0 \pm 4.3, \quad \overset{\circ}{M}_K^2 = 456.2 \pm 20.8. \quad (5.63)$$

From the values of eqs.(5.61) and (5.63) one solves eq.(4.58) for $L_{(7,8)}$ with the result,

$$L_{(7,8)} = -0.6 \pm 0.6, \quad (5.64)$$

in good agreement with typical results in the literature (see table 3), although with large errors.

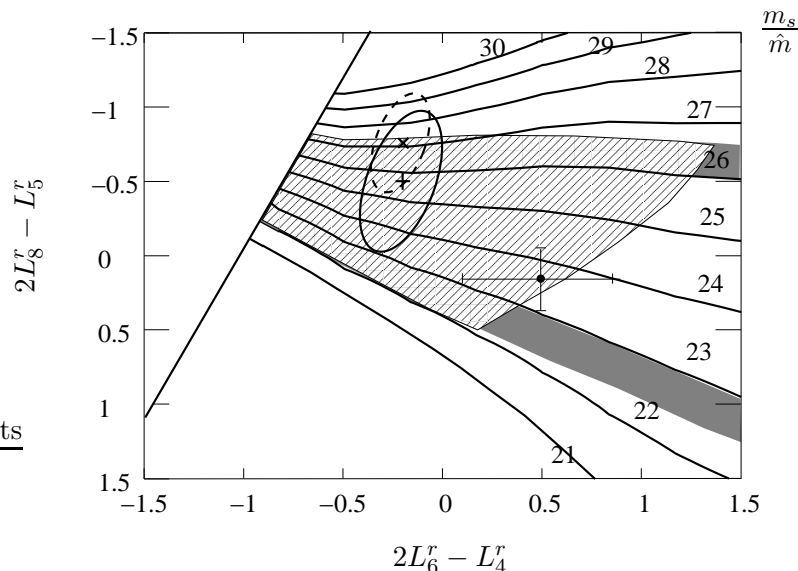


Figure 10: Contour-plot for $r_m = m_s/\hat{m}$ as a function of $L_{(4,6)}$ and $L_{(5,8)}$ showing also our point from the result of the fit to lattice data together with our theoretical uncertainty represented by the solid ellipse. The dashed ellipse represents the value for the LECs, within uncertainty, needed to reproduce the bare masses obtained with the full dynamical model of section 3. On the other hand, the solid point corresponds to the lattice extrapolation from Staggered CHPT [62].

The dashed-ellipse in fig.10 represents the value for the LECs needed to reproduce the results for the bare masses in the full dynamical case of section 3. These values are $2L_8^r - L_5^r = -0.78 \pm 0.25$, $2L_6^r - L_4^r = -0.20 \pm 0.12$. For the latter LEC one gets the same value as in eq.(5.61) while for the

former the central value is almost one sigma smaller than that of eq.(5.61). From there one can conclude that dynamical scalar resonance saturation of $L_{(4,6)}$ is very good but poorer for $L_{(5,8)}$, although still compatible within errors.

On the other hand, it is worth mentioning that in the fit to the unphysical points of lattice the dependence on the bare masses of the pseudoscalar decay constants f_π , f_K and f_η , generally called f_P , could play a role. We have then also performed fits to the lattice data recalculating the f_P in terms of the $\mathcal{O}(p^4)$ CHPT expressions for f_P as a function of the bare masses, with values for L_4^r and L_5^r such that at the physical point the constants f_P have their physical values. As we have checked, these considerations affect little the resulting fit and the results are well within the uncertainty bounds quoted before.

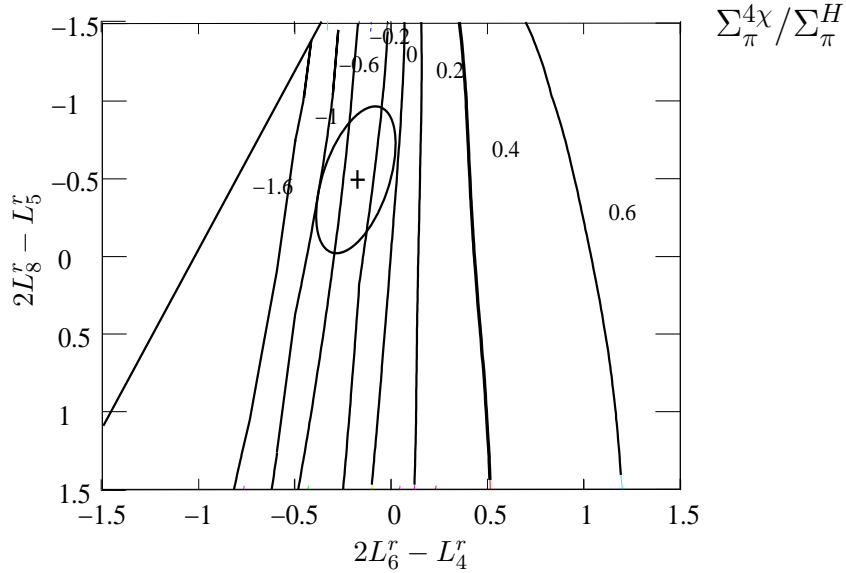


Figure 11: Contour-plots for the ratio of the $\mathcal{O}(p^4)$ CHPT contribution to the pion mass over the $\mathcal{O}(p^6)$ and higher order contribution, as function of $L_{(4,6)}$ and $L_{(5,8)}$.

We also explicitly show in table 4 and in figures 11, 12 and 13 the relative sizes of Σ_P^{4X} and Σ_P^H . In the figures we observe that the ratio between the $\mathcal{O}(p^4)$ and the $\mathcal{O}(p^6)$ and higher order contributions is quite sensitive to the LECs considered. The fact that Σ_P^H is larger than Σ_P^{4X} is in agreement with ref.[57] that performs an $\mathcal{O}(p^6)$ calculation in CHPT of the pseudoscalar masses. Indeed, the sizes of our self-energies from Σ_P^H are rather similar to those determined in this reference to $\mathcal{O}(p^6)$. Ref.[7] obtains: $\Sigma_\pi^{6X}/M_\pi^2 = 0.132 - 0.355$, $\Sigma_K^{6X}/M_K^2 = 0.194 - 0.423$ and $\Sigma_\eta^{6X}/M_\eta^2 = 0.234 - 0.521$. These values are well inside our bulk of results for $\Sigma_\pi^H/M_\pi^2 = 0.222 \pm 0.04$, $\Sigma_K^H/M_K^2 = 0.375 \pm 0.07$, $\Sigma_\eta^H/M_\eta^2 = 0.506 \pm 0.09$. Thus, the calculations of ref.[57] to $\mathcal{O}(p^6)$, although showing that this order is much larger than the $\mathcal{O}(p^4)$, does not imply necessarily the lack of convergence of the chiral series since our calculation, estimating higher orders corrections by incorporating physical S-waves which include both resonant and non-resonant physics, gives us values of similar size to those of this reference up to $\mathcal{O}(p^6)$. We remark that this statement holds only when the $\mathcal{O}(p^6)$ are considered [57] and not for lower orders.

Finally, we have also performed a fit employing only the self-energies calculated at $\mathcal{O}(p^4)$ in CHPT. The result obtained from the fit to lattice data is $2L_8^r - L_5^r = -0.20 \times 10^{-3}$, $2L_6^r - L_4^r = 0.13 \times 10^{-3}$, $3L_7 + L_8^r = -0.08 \times 10^{-3}$ and $m_s/\hat{m} = 28.8$. This value for the quark mass ratio is quite different from our full calculation and much larger than that of ref.[21], stressing again the idea of the important role played by the higher order contributions to the self-energies.

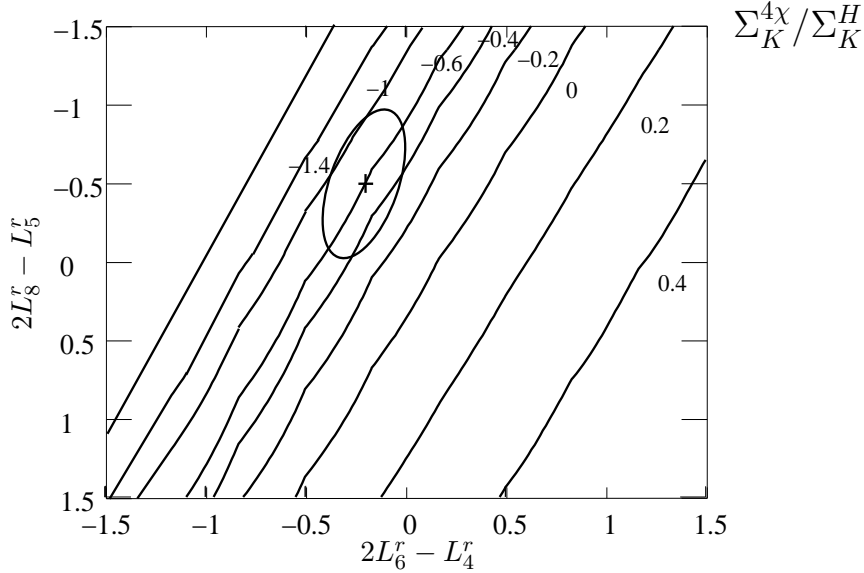


Figure 12: Same as in fig.11 for the kaon.

	π	K	η
$\Sigma_P^{4\chi}/M_P^2$	-0.0789 ± 0.060	-0.221 ± 0.087	-0.410 ± 0.193
Σ_P^H/M_P^2	0.222 ± 0.04	0.375 ± 0.07	0.506 ± 0.09
$\Sigma_P^{4\chi}/\Sigma_P^H$	-0.355 ± 0.287	-0.589 ± 0.236	-0.810 ± 0.384

Table 4: Relative sizes of the $\mathcal{O}(p^4)$, $\mathcal{O}(p^6)$ and higher order contributions, $\Sigma_P^{4\chi}$ and Σ_P^H , respectively, to the self-energies.

6 Conclusions

We have undertaken a non-perturbative chiral study of the self-energies of the lightest pseudoscalar mesons. In their evaluation the S-wave amplitudes obtained in UCHPT, that resum the unitarity cut which is well known to be enhanced and responsible for large higher order chiral corrections, even at low energies, are employed. In this way, our self-energies have accounted for such enhanced diagrams which, among other phenomena, drive to the dynamical generation of the low lying scalar resonances.

The ultraviolet divergences of the scalar self-energy loops have been properly renormalized by sending to infinity a three-momentum cut-off and removing the power like divergences together with the inclusion of a renormalization scale μ . The latter is allowed to vary between 0.5 and 1.2 GeV in order to account for differences in the renormalization scheme. We have made use of a dispersion relation representation of the scattering amplitudes in order to single out analytically the divergent terms in the evaluation of the loops with our full non-perturbative S-waves.

Employing first our approach without matching with the $\mathcal{O}(p^4)$ CHPT self-energies we obtain purely dynamical self-energies. The main conclusion from this part is that most of the physical pseudoscalar masses comes from the bare masses and the dynamical contribution is rather small for the pion and the kaon, although more significant for the eta meson, around 25%.

We then include the $\mathcal{O}(p^4)$ CHPT self-energies and resum the higher order contributions within our approach. Based on the values of the quark mass ratio $m_s/\hat{m} = 24.4 \pm 1.5$ from ref.[21] and values of

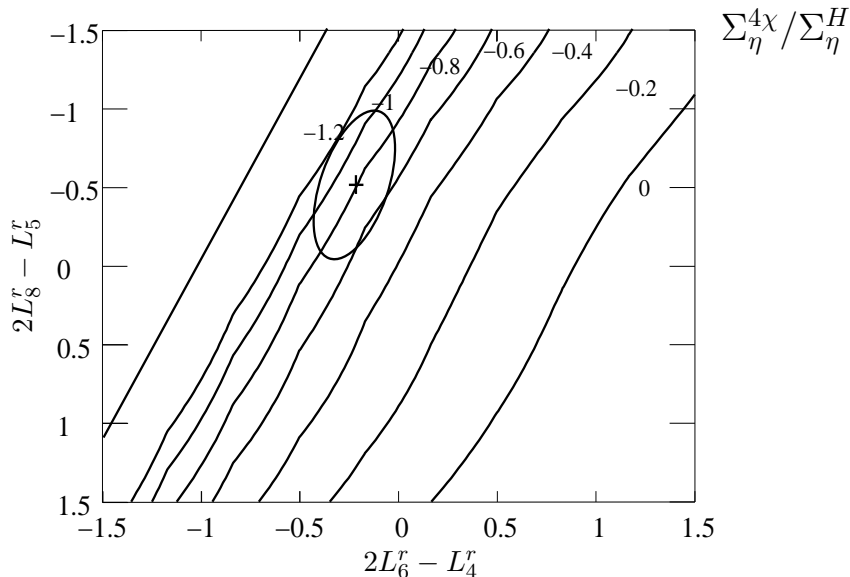


Figure 13: Same as in fig.11 for the eta.

$L_{(7,8)}$ from the literature [61, 57], we have then derived an allowed region for $2L_8^r - L_5^r$ and $2L_6^r - L_4^r$ from the study of the π , K and η masses.

Next, we have given a very good reproduction of the three dynamical fermion lattice data on the pseudoscalar masses from the MILC Collaboration [17] at the level of 1.2% error. We then obtain from our non-perturbative chiral extrapolation $m_s/\hat{m} = 25.6 \pm 2.5$, that has a central value compatible with that of ref.[21], previously given. This shows that the MILC data on the pseudoscalar masses do not necessarily imply the significantly larger value, 27.4 ± 0.5 [18], for m_s/\hat{m} than that of ref.[21]. We have also derived from the fit to lattice data the values $2L_8 - L_5 = -0.5 \pm .05$ and $2L_6 - L_4 = -0.2 \pm 0.17$ in units of 10^{-3} for the $\mathcal{O}(p^4)$ CHPT LECs, well inside the region previously favoured.

Other interesting result from our investigation is that although the $\mathcal{O}(p^6)$ contribution to the self-energies calculated in three flavour CHPT [7] is much larger than the $\mathcal{O}(p^4)$ one, we still obtain self-energies of similar values to those of ref.[7] including our estimated higher order corrections. This seems to indicate that the chiral expansion in the calculation of the self-energies is not spoiled and the values obtained tend to stabilize once the $\mathcal{O}(p^6)$ is taken into account.

Acknowledgements

We would like to thank Urs M. Heller for useful communications and discussions. Financial support by MEC (Spain) grants No. FPA2004-03470, No. BFM-2003-00856, Fundaci3n S3neca (Murcia) grant Ref. 02975/PI/05, the European Commission (EC) RTN Program Network ‘‘EURIDICE’’ Contract No. HPRN-CT-2002-00311 and the HadronPhysics I3 Project (EC) Contract No. RII3-CT-2004-506078 is acknowledged.

References

- [1] S. Weinberg, *Physica* **A96** (1979) 327.

- [2] J. Gasser and H. Leutwyler, *Ann. Phys.* **158** (1984) 142.
- [3] J. Gasser and H. Leutwyler, *Nucl. Phys.* **B250** (1985) 465.
- [4] J. Bijnens, G. Colangelo and G. Ecker, *JHEP* **9902** (1999) 020.
- [5] J. Bijnens, G. Colangelo and G. Ecker, *Annals Phys.* **280** (2000) 100.
- [6] J. Bijnens, *AIP Conf. Proc.* **698** (2004) 407, and references therein.
- [7] G. Amoros, J. Bijnens and P. Talavera, *Nucl. Phys.* **B568** (2000) 319.
- [8] B. Ananthanarayan, G. Colangelo, J. Gasser and H. Leutwyler, *Phys. Rept.* **353** (2001) 207; G. Colangelo, J. Gasser and H. Leutwyler, *Phys. Lett.* **B488** (2000) 261; I. Caprini, G. Colangelo, J. Gasser and H. Leutwyler, *Phys. Rev.* **D68** (2003) 074006.
- [9] S. Descotes-Genon, N. H. Fuchs, L. Girlanda and J. Stern, *Eur. Phys. J.* **C24** (2002) 469.
- [10] J. R. Pelaez and F. J. Yndurain, *Phys. Rev.* **D71** (2005) 074016; *Phys. Rev.* **D68** (2003) 074005; R. Kaminski, J. R. Pelaez and F. J. Yndurain, arXiv:hep-ph/0603170.
- [11] J. Gasser and H. Leutwyler, *Nucl. Phys.* **B250** (1985) 539.
- [12] C. Roiesnel and T. N. Truong, *Nucl. Phys.* **B187** (1981) 293; T. N. Truong, *Phys. Rev. Lett.* **61** (1988) 2526; *Phys. Lett.* **B207** (1988) 495.
- [13] J. A. Oller and E. Oset, *Nucl. Phys.* **A620** (1997) 438; (E)-*ibid.* **A652** (1999) 407.
- [14] J. A. Oller and E. Oset, *Phys. Rev.* **D60** (1999) 074023.
- [15] M. Jamin, J. A. Oller and A. Pich, *Nucl. Phys.* **B587** (2000) 331
- [16] A. Dobado and J. R. Pelaez, *Phys. Rev.* **D56** (1997) 3057.
- [17] C. Aubin *et al.*, *Phys. Rev.* **D70** (2004) 094505.
- [18] C. Aubin *et al.*, *Phys. Rev.* **D70** (2004) 031504.
- [19] Q. Mason, H. D. Trottier, R. Horgan, C. T. H. Davies and G. P. Lepage [HPQCD Collaboration], *Phys. Rev.* **D73** (2006) 114501
- [20] W. J. Lee and S. R. Sharpe, *Phys. Rev.* **D60** (1999) 114503; C. Bernard [MILC Collaboration], *Phys. Rev.* **D65**, 054031 (2002); C. Aubin and C. Bernard, *Phys. Rev.* **D68** (2003) 034014.
- [21] H. Leutwyler, *Phys. Lett.* **B378** (1996) 313.
- [22] J. A. Oller, E. Oset and J. R. Pelaez, *Phys. Rev. Lett.* **80** (1998) 3452; *Phys. Rev.* **D59** (1999) 074001; (E)-*ibid.* **D60** (1999) 099906.
- [23] J. A. Oller and E. Oset, *Nucl. Phys.* **A629** (1998) 739.
- [24] U. G. Meissner and J. A. Oller, *Nucl. Phys.* **A679** (2001) 671; T. A. Lahde and U. G. Meissner, arXiv:hep-ph/0606133.
- [25] J. A. Oller, E. Oset and J. E. Palomar, *Phys. Rev.* **D63** (2001) 114009.

- [26] M. Jamin, J. A. Oller and A. Pich, Nucl. Phys. **B622** (2002) 279.
- [27] J. A. Oller, Phys. Lett. **B426** (1998) 7; Nucl. Phys. **A714** (2003) 161; J. E. Palomar, L. Roca, E. Oset and M. J. Vicente Vacas, Nucl. Phys. **A729** (2003) 743.
- [28] L. Roca, J. E. Palomar, E. Oset and H. C. Chiang, Nucl. Phys. **A744** (2004) 127.
- [29] E. Oset, J. R. Pelaez and L. Roca, Phys. Rev. **D67** (2003) 073013.
- [30] S. Gardner and U. G. Meissner, Phys. Rev. **D65** (2002) 094004; U. G. Meissner and S. Gardner, Eur. Phys. J. **A18** (2003) 543; J. A. Oller, eConf **C0304052** (2003) WG412.
- [31] J. A. Oller, Phys. Rev. **D71** (2005) 054030.
- [32] M. Jamin, J. A. Oller and A. Pich, JHEP **0402** (2004) 047; Eur. Phys. J. **C24** (2002) 237; arXiv:hep-ph/0605095.
- [33] G. Ecker, J. Gasser, A. Pich and E. de Rafael, Nucl. Phys. **B321** (1989) 311.
- [34] S. Eidelman *et al.* [Particle Data Group], Phys. Lett. **B592** (2004) 1.
- [35] J. A. Oller and U. G. Meissner, Phys. Lett. **B500** (2001) 263.
- [36] J. A. Oller, Phys. Lett. **B477** (2000) 187.
- [37] B. Hyams *et al.*, Nucl. Phys. B 64 (1973) 134; P. Estrabooks *et al.*, AIP Conf. Proc. 13 (1973) 37; G. Grayer *et al.*, Proc. 3rd Philadelphia Conf. on Experimental Meson Spectroscopy, Philadelphia, 1972 (American Institute of Physics, New York, 1972) 5; S.D. Protopopescu and M. Alson-Garnjost, Phys. Rev. D 7 (1973) 1279.
- [38] R. Kaminski, L. Lesniak and K. Rybicki, Z. Phys. C 74 (1997) 79.
- [39] W. Ochs, University of Munich, thesis, 1974.
- [40] C.D. Froggatt and J.L. Petersen, Nucl. Phys. B 129 (1977) 89.
- [41] D. H. Cohen, D. S. Ayres, R. Diebold, S. L. Kramer, A. J. Pawlicki and A. B. Wicklund, Phys. Rev. D **22** (1980) 2595.
- [42] A. Etkin *et al.*, Phys. Rev. D 28 (1982) 1786.
- [43] W. Wetzel *et al.*, Nucl. Phys. B 115 (1976) 208; V.A. Polychronakos *et al.*, Phys. Rev. D 19 (1979) 1317; G. Costa *et al.*, Nucl. Phys. B 175 (1980) 402.
- [44] R. Mercer *et al.*, Nucl. Phys. B 32 (1971) 381.
- [45] P. Estabrooks, R. K. Carnegie, A. D. Martin, W. M. Dunwoodie, T. A. Lasinski and D. W. G. Leith, Nucl. Phys. B **133**, 490 (1978).
- [46] T.A. Armstrong *et al.*, Z. Phys. C 52 (1991) 389.
- [47] D. Linglin *et al.*, Nucl. Phys. B **57** (1973) 64.
- [48] A. D. Martin and E. N. Ozmutlu, Nucl. Phys. B **158** (1979) 520.

- [49] L. Rosselet et al., Phys. Rev. D **15** (1997) 574.
- [50] J. A. Oller and U.-G. Meißner, Phys. Lett. **B500** (2000) 263.
- [51] J. A. Oller, J. Prades and M. Verbeni, Phys. Rev. Lett. **95** (2005) 172502.
- [52] J. A. Oller, Eur. Phys. J. **A28** (2006) 63.
- [53] R. F. Dashen, Phys. Rev. **183** (1969) 1245.
- [54] J. F. Donoghue, B. R. Holstein and D. Wyler, Phys. Rev. **D47** (1993) 2089.
- [55] R. Urech, Nucl. Phys. **B433** (1995) 234.
- [56] J. Bijnens and J. Prades, Nucl. Phys. **B490** (1997) 239.
- [57] G. Amoros, J. Bijnens and P. Talavera, Nucl. Phys. **B585** (2000) 293; (E)-ibid. **B598** (2001) 665.
- [58] N. H. Fuchs, H. Sazdjian and J. Stern, Phys. Lett. B **269** (1991) 183; J. Stern, H. Sazdjian and N. H. Fuchs, Phys. Rev. D **47** (1993) 3814.
- [59] G. Ecker, J. Gasser, A. Pich and E. de Rafael, Nucl. Phys. **B321** (1989) 311.
- [60] B. Ananthanarayan, P. Buettiker and B. Moussallam, Eur. Phys. J. **C22** (2001) 133.
- [61] J. Bijnens, G. Colangelo and J. Gasser, Nucl. Phys. **B427** (1994) 427.
- [62] C. Aubin *et al.* [MILC Collaboration], Phys. Rev. **D70** (2004) 114501